Friction **12**(3): 396–427 (2024)
https://doi.org/10.1007/s40544-023-0761-7
ISSN 2223-7690
CN 10-1237/TH

REVIEW ARTICLE

Advances in friction of aluminium alloy deep drawing

Yiren GAO, Hongxia LI*, Danyang ZHAO, Minjie WANG, Xiaobo FAN
School of Mechanical Engineering, Dalian University of Technology, Dalian 116023, China
Received: 11 February 2022 / Revised: 22 August 2022 / Accepted: 21 March 2023

Abstract: Broad use of lightweight aluminium alloy parts in automobile manufacturing, aerospace, electronic communication, and rail transit is mainly formed through deep drawing process. Deep drawing friction is a key boundary condition for controlling the forming quality of aluminium alloy parts. However, due to the oxidation and adhesion tendency of aluminium alloys, the tribological situations of aluminium alloy deep drawing (AADD) system is more complicated than those of traditional deep drawing of steel sheets. Therefore, the study of AADD friction is essential for manufacturing high-performance aluminium alloy parts. Herein, aiming to provide a valuable reference for researchers in related fields, a comprehensive review of AADD friction is provided, including friction mechanism, influencing factors, friction measurement, friction model, friction simulation, and lubrication-free friction control. Finally, a brief conclusion and several current challenges were discussed.

Keywords: aluminium alloy deep drawing (AADD); influencing factors; friction measurement; friction model; friction control

1 Introduction

Aluminium alloys are known to be the lightweight alloys that offer high specific strength and stiffness together with good weldability, machinability, and corrosion resistance [1]. As the demand for lightweight industrial products continues to increase, aluminium alloys showed promising applications in automobile manufacturing, aerospace, electronic communications, and rail transit. Currently, aluminium alloy sheets are mainly formed through deep drawing process, not only because of its high machining efficiency, but also because that it enables manufacturing components with complex geometry. However, the surfaces of die and aluminium alloy sheets are not ideally smooth, and there are complex interactions at the contact interface during the deep drawing process, forming a multi-variable and time-varying tribological system. The friction between die and the aluminium alloy sheets plays a decisive role in controlling the ultimate quality of the sheets by affecting the material flow and the interface stress and strain distribution. Therefore, fully understanding the tribological behavior in deep drawing process is critical to improving the performance of aluminium alloy parts.

To reduce the lost time and manufacturing costs due to try-out and design changes of die, it is essential to establish friction models that accurately predict the actual deep drawing process in the early stage of product development. By quantifying the contributions of different factors of a tribological system to friction behavior, friction models can evaluate the robustness of an industrial production process. Using friction models to investigate possible scenarios corresponding to production conditions prior to the final design and machining of the die can contribute to determining a robust process window to obtain defect-free parts. However, the interface friction behavior in the deep drawing process changes with the variations of lubrication amount, lubrication distribution, and die

* Corresponding author: Hongxia LI, E-mail: hxli@dlut.edu.cn

temperature, and it is difficult to guarantee the quality of parts during continuous production for a long time. This requires control and regulation of the friction to control the process. In 2018, Tatipala et al. [2, 3] analyzed the influence of lubrication performance changes on the quality of the front door inner of a Volvo XC90 based on the lubrication amount and lubrication distribution data measured in production, which improved the prediction accuracy of the part forming performance. In 2020, Veldhuis et al. [4, 5] studied the sensitivity of the process to temperature-induced frictional effects, and adjusted the blank holder force F_H and ejection force in real time to adapt the process to the tribological system changes caused by die heating, thereby avoiding the fracture caused by the deterioration of friction conditions. Thus, building the link between the control systems based on friction models and the manufacturing technologies can realize stable process control to improve the quality of deep drawing parts and the overall production stability.

To study the important role of friction in sheet metal forming, some excellent review papers on metal forming friction have been published in recent decades. As early as 1986, Kalpakjian [6] outlined the importance and complexity of tribology in sheet metal forming. Subsequently, Kawai and Dohda [7] listed the friction test methods suitable for sheet metal forming, focusing on the influence of different factors on the lubrication mechanism. In 2003, Guo et al. [8] summarized the friction models commonly used in simulation of sheet metal stamping. In 2014, Meng et al. [9] divided the existing friction models into five categories based on the development of friction models in metal plastic forming, and the characteristics of various friction models and their application scopes were discussed in detail. In 2018, Seshacharyulu et al. [10] and Xu et al. [11] briefly introduced several devices to measure the coefficient of friction (COF) μ, and analyzed the influence of process parameters on the friction law by investigating the friction characteristics in sheet plastic forming. In 2018, Nielsen and Bay [12] took time as the boundary and summarized the important progress of friction modelling in the metal forming process (1942–2016) since Bowden and Tabor [13] put forward the adhesion theory. Li et al. [14] reviewed the friction mechanism and the influencing factors of friction characteristics in the stamping process. In 2020, Trzepiecinski and Lemu [15] classified and summarized the friction test apparatus of conventional sheet metal forming and incremental sheet forming in detail. Although these reviews analyzed sheet forming friction from multiple angles, they mainly targeted at traditional steel sheet forming and cannot fully reflect the complex tribological conditions in the aluminium alloy deep drawing (AADD) process. To date, review papers systematically elucidating AADD friction have not been reported.

Different from steel, aluminium alloys exhibit poor formability at room temperature due to lower tensile strength and elongation at break [16]. In addition, when hard die is in contact with soft aluminium sheet, the surface of aluminium sheet will undergo severe plastic deformation, and the surface material will detach and transfer from the substrates. Aluminium chips are easy to adhere to die surface. Accompanied by the oxidation reaction that might occur, a transfer layer with complex compositions will be formed [17]. Because of the significant adhesion between the die and the aluminium alloy sheet, the AADD system has unique friction characteristics. Therefore, a comprehensive review of AADD from friction mechanism to friction control will provide a valuable reference for researchers in related fields.

The organizational structure of this review is shown in Table 1. Section 1 introduces the background of AADD friction. Section 2 analyzes the friction behavior of AADD and its influencing factors. Section 3 reports the friction test methods of AADD. Section 4 summarizes the friction models of AADD, including empirical models based on friction test results and

Table 1 Organizational structure of this review.

Section	Content
1	Background of AADD friction
2	Friction behavior of AADD and its influencing factors
3	Friction test methods of AADD
4	Friction models of AADD
5	Friction simulation methods of AADD
6	Lubrication-free technologies in controlling AADD friction
7	Conclusion and challenges of AADD friction

theoretical models derived from the friction theory. Section 5 explains the friction simulation methods of AADD based on friction test and friction model. Section 6 emphasizes the role of lubrication-free technologies such as solid lubrication, surface texture, and coating modification in controlling AADD friction and improving the performance of aluminium alloy parts. Section 7 draws a brief conclusion and discusses several current challenges of AADD friction.

2 AADD friction

The friction between the die and the aluminium alloy sheet affects the interface force, inhibits the material flow, and regulates the sheet deformation behavior during the deep drawing process. But friction is not an isolated state; it depends on the complex interactions of rough surfaces, and is affected by many factors such as deep drawing process parameters, die–sheet surface and material characteristics, and lubrication conditions. In Section 2, the influence of friction behavior on AADD is discussed, and the influencing factors of AADD friction are analyzed.

2.1 Influence of friction on AADD

Under F_H, punch force F_D, and friction force f, the aluminium alloy sheet will undergo large plastic deformation during the deep drawing process. The stress and strain states of different regions of sheet exhibit remarkable differences. This is illustrated in Fig. 1. The sheet deformation zone is mainly divided into nine regions: I, blank holder region; II, drawbead region; III, inner ring region; IV, die radius region; V, straight wall region; VI, punch outer radius region; VII, punch outer flat region; VIII, punch inner radius region; and IX, punch inner flat region. The blank holder, drawbead, and inner ring regions are the primary deformation zone. Under F_H, friction forces f_1, f_2, f_3, f_4, f_5, and f_6 that inhibit the material flow were generated separately for blank holder–sheet and die–sheet interface. Internal material subjected to the radial tensile stress σ_r, tangential compressive stress σ_θ, and thickness compressive stress σ_t, which generate radial tensile strain ε_r, tangential compressive strain ε_θ, and thickness compressive strain ε_t. The die radius region is the transitional zone, where blank holder, drawbead, and inner ring region material enter the straight wall region. Under die radius region pressure and friction force f_7, internal material subjected to σ_r, σ_θ, and σ_t. The straight wall region is the force transmission zone. Due to the gap between die, punch, and sheet, internal material only subjected to σ_r and σ_θ. The punch outer radius region is the transitional zone between punch outer flat, inner radius, inner flat regions, and straight wall region. Under punch outer radius region pressure and friction force f_8, internal material subjected to σ_r, σ_θ, and σ_t. The punch outer flat, inner radius, and inner flat regions are the primary forming zone. Under F_D, friction forces f_9, f_{10}, and f_{11} that inhibit the material flow were generated separately for punch–sheet and die–sheet interface. Internal material subjected to σ_r and σ_θ, and compressive strain occurs in thickness direction.

AADD friction is mostly controlled by the friction distribution of flange region (blank holder, drawbead, and inner ring regions), die radius region, and punch

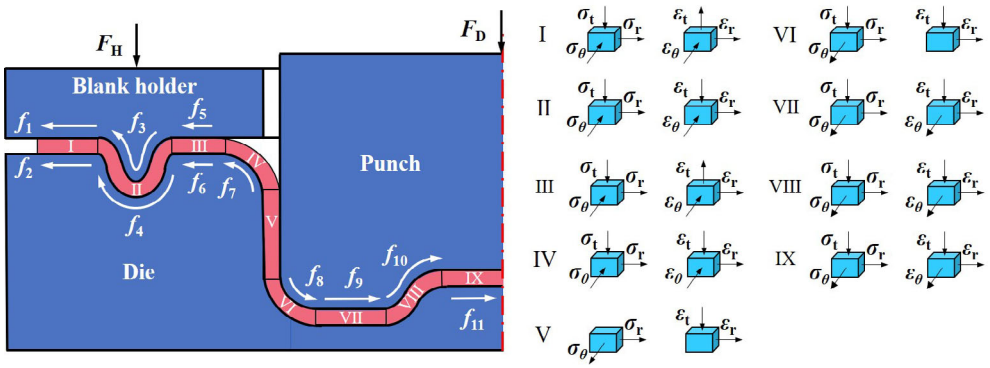

Fig. 1 Stress and strain states of AADD: I, blank holder region; II, drawbead region; III, inner ring region; IV, die radius region; V, straight wall region; VI, punch outer radius region; VII, punch outer flat region; VIII, punch inner radius region; and IX, punch inner flat region.

radius region, which affects the stress and strain states of different regions of sheet and the forming performance of parts. Bouchaâla et al. [18] studied the impact of friction on the wall thickness distribution of AA2198 deep drawing parts by contrasting the simulation and experimental results. Reddy et al. [19] investigated the effect of COF on the limit drawing ratio and limit strain of AA1100, and found that the limit drawing ratio and limit strain of the workpiece decrease with the increase of the COF. Folle and Schaeffer [20] showed that the COF in AA1100 deep drawing process is not a constant value, and the variations of COF affect the drawing force. Bellini et al. [21] analyzed the influence of friction on the forming properties of AA6060 discs. The deep drawing tests and simulations of AA6111 by Ma et al. [22] and AA 6061-T4 by Mohamed et al. [23] also confirmed that friction is a key factor affecting the thickness, forming limit, maximum thinning position, and failure modes of parts.

2.2 Influencing factors of AADD friction

As shown in Fig. 2, friction is a bridge linking the influencing factors of deep drawing system and the forming quality of parts. The unreasonable friction distribution will cause wrinkling, fracture, springback, and other defects. These can be attributed to the influence of different input factors on AADD friction. However, the difficulty of AADD frictional study lies in that as the input conditions vary, the proportion of different factors will change, and the law might also be completely opposite.

2.2.1 Process parameters

AADD friction has a strong correlation with temperature. So far, reports related to AADD friction have mainly focused on conventional cold deep drawing and hot deep drawing. Lu et al. [24, 25] revealed the friction mechanism of AA7075 sheet at different temperatures. When the temperature is lower than 150 °C, plowing friction dominates; and when the temperature is higher than 300 °C, adhesive friction dominates. In the temperature range of 25–450 °C, Hanna [26] and Gali et al. [27] carried out the P20 and AA5083 friction test, respectively. Although the COF increases with the increase of temperature, there is a large difference of tendency between them. The COF of the former only changes drastically at 200–300 °C, while the COF of the latter increases exponentially with the increase of temperature. In the 300–500 °C temperature range, the friction test of AA6061 by Liu et al. [28] and AA6111 by Dou et al. [29] also obtained similar changes. Although warm/hot deep drawing improves the forming properties of aluminium alloys, this operation may affect the microstructures and mechanical behaviors of aluminium alloys. Because the cryogenic temperature can significantly improve the strength and toughness of aluminium alloys, and the parts have good comprehensive performance. In the past seven years, the cryogenic temperature deep drawing of aluminium alloy sheet (Fig. 3) has received a massive amount of interest [1, 30–34]. In contrast, there is a lack of research on cryogenic temperature AADD friction. In 2019, only Padmini et al. [35] conducted AA2024, AA6082, and AA7075 cryogenic temperature friction tests at −196 °C in liquid nitrogen, and found that cryogenic temperature environments can reduce COF and improve the tribological properties of aluminium alloys.

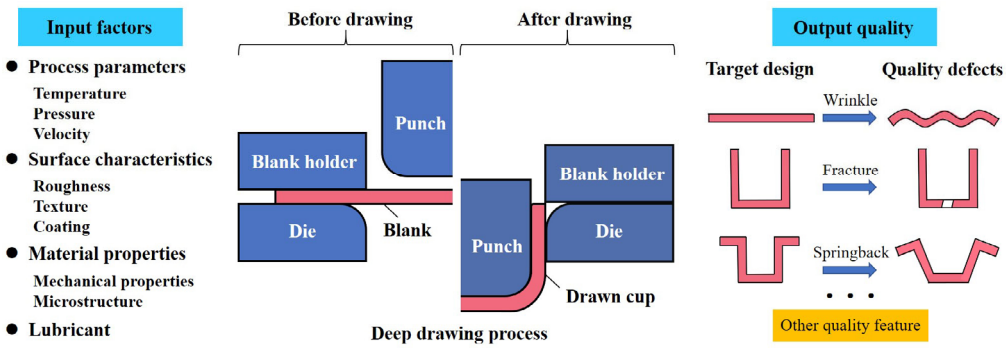

Fig. 2 Influencing factors of AADD friction on forming quality of parts.

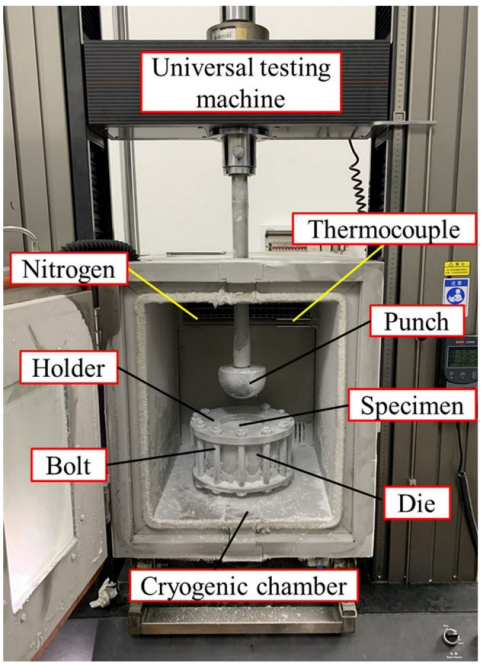

Fig. 3 AADD at cryogenic temperatures. Reproduced with permission from Ref. [34], © The Korean Institute of Metals and Materials 2021.

Under different contact pressures and velocities, AADD friction undergoes marked changes. The AA3004 dry friction test of Lin et al. [36] showed that under low pressures, increasing the drawing speed can reduce friction. When the pressure is large enough, the effect of drawing speed on friction is weakened. Under lubrication conditions, the friction tests of AA5023 by Ooki and Takahashi [37], AA6063 by Hwang and Chen [38], and AA5182 and AA6016 by Sabet et al. [39] showed that the larger the sliding speed, the smaller the COF. However, the AA6014 friction test of Steiner and Merklein [40] pointed out that the drawing speed is not related to friction under dry contact conditions, and the COF increases with the increase in contact pressure (the same conclusion as that reported in Refs. [25, 28]). The drawing speed affects the friction under lubrication conditions, and the COF decreases with the increase of contact pressure (the same conclusion as that reported in Refs. [39, 41, 42]). Contrary to those reported in Refs. [25, 28, 40], the dry friction test of 1.2343/AA6016 by Domitner et al. [43] showed that the COF decreases with the increase of contact pressure. In the P20/AA7075 friction test conducted by Yang et al. [44], when the system is in a boundary lubrication condition, the influence of contact pressure and sliding speed on friction can be ignored. The friction test of Shi et al. [45] confirmed it. Due to the extremely complicated influence of the deep drawing process on the AADD friction, single conclusion cannot truly reflect the friction behavior of contact interface.

2.2.2 *Surface characteristics*

AADD friction is affected by the surface roughness, coating, and texture of sheets and tools. Aluminium alloy sheet is commercially available in three surface finishes, i.e., milling finish (MF), dull finish (DF), and electrical discharge texturing (EDT). Among them, MF has the lowest surface roughness, and EDT has the highest surface roughness [46]. The surface morphologies of MF and EDT aluminium alloy sheets are shown in Fig. 4 [47]. Under lubrication conditions, Keum et al. [48] found that when the surface roughness of aluminium alloy sheet is low, the COF decreases with the increase of surface roughness due to small cavity for storing lubricating oil. When the surface roughness of aluminium alloy sheet is high, the oil film ruptures due to surface asperity plastic deformation, and the COF increases with the increase of the surface roughness. Lemu and Trzepieciński [49] pointed out that the influence of tool surface roughness on friction depends on the friction conditions (dry or lubrication conditions). Under dry friction conditions, tools with low surface roughness may not necessarily reduce friction. Under lubrication conditions, the law is the same as that reported in Ref. [48]. In addition, coatings can reduce AADD friction and forming force under dry conditions [50–52]. Steiner et al. [53] conducted friction test between 1.2379-coated tools and AA5182, and the results showed that the lower

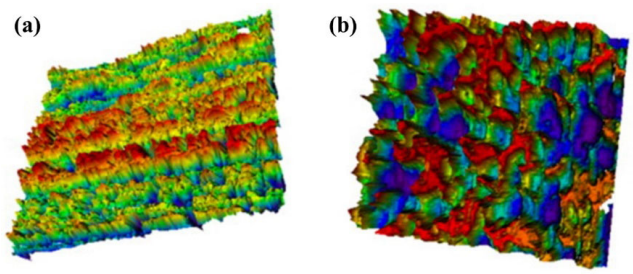

Fig. 4 Surface morphologies of aluminium alloy sheets: (a) MF sheet; (b) EDT sheet. Reproduced with permission from Ref. [47], © Elsevier B.V. 2011.

the surface roughness of coated tools, the smaller the COF. Abraham et al. [51] further corroborated that the low surface roughness of coated tools is beneficial to reducing adhesive friction of AA5083. The aluminium alloy sheet is affected by the manufacturing process, and the surface roughness also has obvious orientation characteristics. Aktürk et al. [54] proposed that the COF is the smallest when sliding parallel to the rolling direction of AA6111 sheet. However, the conclusions of Liu et al. [55] and Saha et al. [56] are completely opposite to that reported in Ref. [54]. Menezes et al. [57, 58] believed that the COF is not relevant in the surface roughness, but is relevant in the surface texture of tool. Zabala et al. [59] analyzed the friction behavior between GGG70 tools with different polishing degrees and AA1050 sheets with different degrees of EDT textures under lubrication conditions. The results showed that the COF decreases with the increase of texture degree of aluminium alloy sheet and increases with the increase of tool roughness. Therefore, only combining specific tribological conditions can the influence of surface characteristics on AADD friction be correctly analyzed.

2.2.3 *Material properties*

AADD friction involves sophisticated elastoplastic deformation of the die–sheet surface. This is closely related to the mechanical properties, microstructures, and material transfer of the contact process. It can be seen from Fig. 5(a) that the surface hardness of aluminium alloys is significantly less than that of tool steel. The plastic deformation of aluminium pin tip gradually increases with the increase of sliding distance $\overline{u}^s$ [17]. The scratches during the friction process cause the aluminium alloy detachment from surface, which is easy to adhere to tool (Fig. 5(b)), forming a material transfer layer. The transfer layer on tool surface interacts with the oxide layer on sheet surface, which increases the friction between tool and sheet [43]. Hu et al. [60] studied the formation mechanism of aluminium transfer layer on cast iron (CI) and the evolution of the friction system from transition state to steady state through the G3500/AA6082 dry friction test. Wilson and Sheu [61] proposed that the effective hardness of sheet surface is substantially reduced due to plastic flow. The friction test of Keum et al. [48] indicated that with the increase of surface hardness of aluminium alloy sheet, the COF decreases slightly. Zhao et al. [62] discussed the dry friction mechanism of closed and open friction systems. In a closed system, AA5182 with higher yield strength and lower elongation shows higher adhesion. In an open system, since loose abrasive particles can be separated from the contact interface, adhesive friction is reduced.

Microstructure is another important factor affecting AADD friction. For this reason, Afshin and Kadkhodayan [63] determined the COFs of AA1050 and AA5052 sheets at different grain sizes by Coulomb friction test. The results showed that the COF increases with the increase of grain size. Lu et al. [24, 25] established the AA7075 hard phase dissolution–precipitation coupled friction evolution model (Fig. 6) by analyzing the role of hard phase of microstructure, oxides, and wear debris in friction process. In contrast, Kirkhorn et al. [64] analyzed the influence of tool steel microstructure on sheet forming friction. And they found that there is no direct link between the amount of carbide precipitation and the COF. Since the material properties directly affect the force and

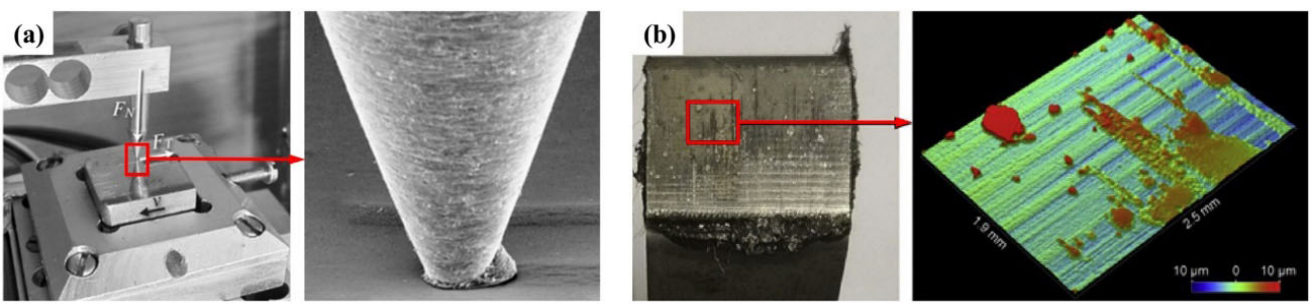

Fig. 5 (a) Tip deformation of soft aluminium; (b) aluminium adhesion on hard tool during friction process. Note: v is the sliding velocity. Reproduced with permission from Ref. [17] for (a), © The Author(s) 2018; Ref. [43] for (b), © The Authors 2021.

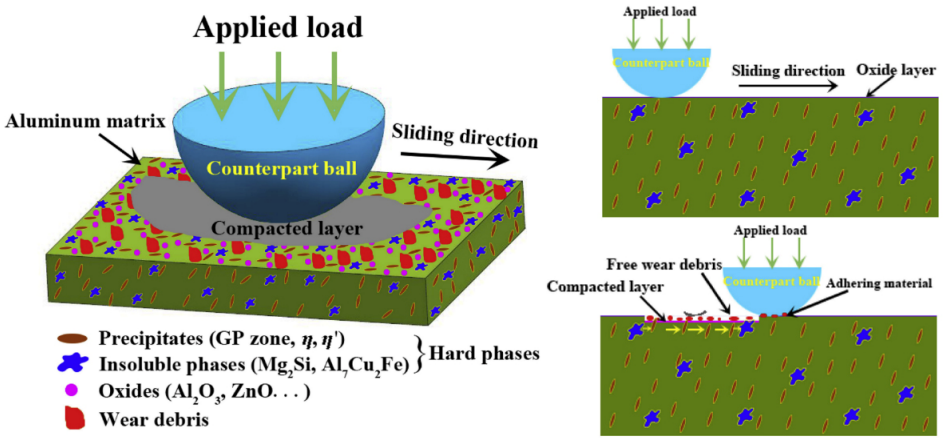

Fig. 6 Friction evolution model based on AA7075 microstructure hard phase dissolution–precipitation coupling. Reproduced with permission from Ref. [24], © Elsevier Ltd. 2019.

deformation of contact interface, it is vital for the in-depth analysis of the AADD friction mechanism.

2.2.4 *Lubrication*

Lubrication can directly change the contact conditions of solid surface. It is an important means to reduce AADD friction. Lin et al. [36] and Keum et al. [48] studied the effect of lubricating oil viscosity on AADD friction. And the results showed that the COF decreases with the increase of lubricating oil viscosity. Yang et al. [44] further studied the influence of oil film thickness and concluded that the COF increases with the decrease of oil film thickness. Meiler and Jaschke [65] compared the lubricating properties of liquid lubricants and dry film lubricants. It is found that the dry film lubricant is evenly distributed on the surface of aluminium alloy sheet during deep drawing process, which is more beneficial to improving the friction conditions of contact interface and the formability of sheet. Because traditional liquid lubricants contain harmful ingredients. Dyja and Więckowski [66] developed a biodegradable liquid lubricant to reduce AA2024 friction.

3 Friction measurement

Under the complex influencing factors of deep drawing system, the friction phenomenon, law, and mechanism of AADD exhibit large uncertainties. For this, the development of friction measurement methods suitable for deep drawing is of great significance for studying the friction behavior and estimating the COF. Because of the different friction characteristics in different regions, it is currently impossible using a single friction test to characterize the ever-changing sheet forming conditions. Figure 7 summarizes the main friction measurement methods for three typical regions, including flange region, die radius region, and punch radius region.

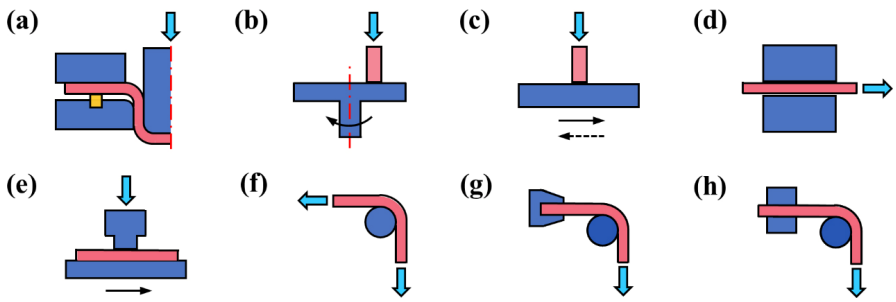

Fig. 7 COF measurement methods for deep drawing: (a) *in-situ* friction measurement; (b) rotary pin-on-disk tribometer; (c) reciprocating pin-on-disk tribometer; (d) strip drawing test; (e) strip sliding test; (f) bending under tension (BUT) (die radius); (g) BUT (punch radius); and (h) compound friction test.

3.1 Friction measurement in flange region

3.1.1 *In-situ friction measurement*

The *in-situ* measurement technology (Fig. 7(a)) can obtain F_H and tangential force T simultaneously by installing a force sensor on die surface, and directly determine the μ during the deep drawing process. The existing *in-situ* friction measurement methods include the probe sensor measurement method (Fig. 8(a)) and the three-axis force sensor measurement method (Fig. 8(b)) [67–69]. The *in-situ* measurement can reflect the real COF of flange region, but the installation of sensors exists inherent limitations, and it cannot be installed in the radius region of die or punch.

3.1.2 *Pin-on-disk tribometer*

The rotary pin-on-disk tribometer (Fig. 7(b)) and the reciprocating pin-on-disk tribometer (Fig. 7(c)) are two common COF measurement methods. Wang et al. [70] improved the cylindrical pin to rectangular pin, which increases the contact area between the pin and disk, and reduces the possibility of the local eccentric load under a small contact area. Dong et al. [71] and Hanna [26] used a reciprocating pin-on-disk tribometer to study AADD friction and aluminium adhesion. Yang et al. [44] used a robot to measure the friction between the tool pin and the aluminium alloy sheet under variable contact conditions. Compared with the actual forming conditions, repeated contact between the pin and disk will change the friction conditions and affect the measurement results.

3.1.3 *Strip drawing test*

The strip drawing test (Fig. 7(d)) can simulate the friction behavior of flange region. The test uses upper and lower tool blocks, clamps the metal strip under F_H, and slides the metal strip along tool surface through T. The calculation method of the μ is shown in Eq. (1).

$$\mu = \frac{T}{2F_H} \tag{1}$$

As shown in Figs. 9(a)–9(d), Recklin et al. [69]

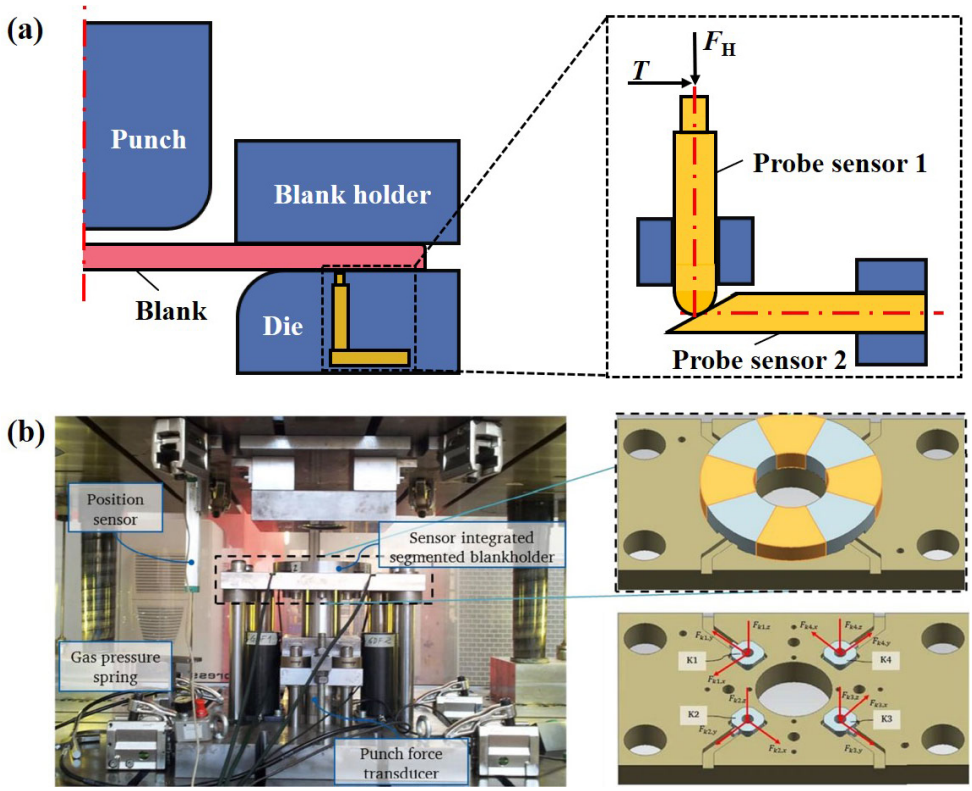

Fig. 8 COF *in-situ* measurement: (a) probe sensor measurement; (b) three-axis force sensor measurement. Reproduced with permission from Ref. [69] for (b), © IOP Publishing Ltd 2017.

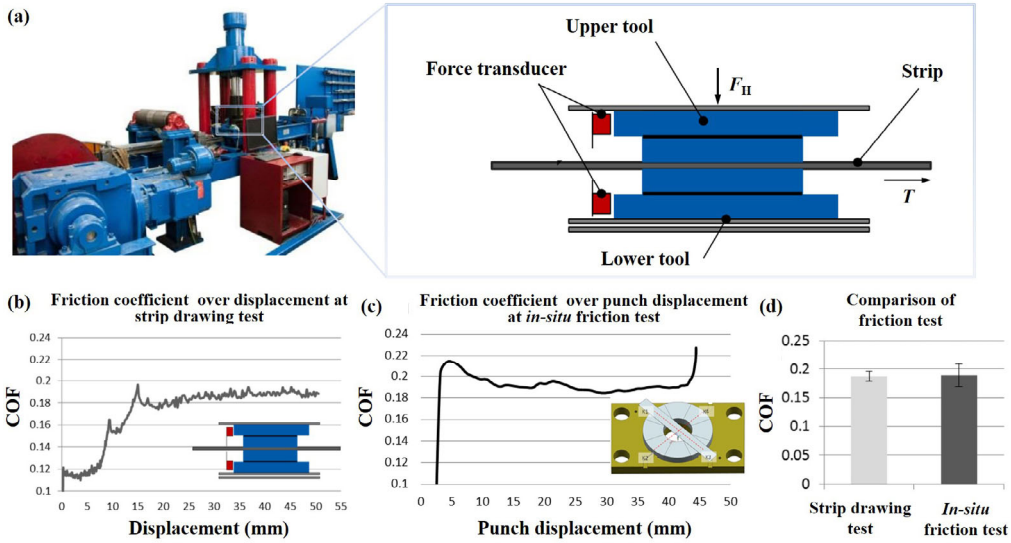

Fig. 9 (a) Strip drawing test apparatus; (b) strip drawing test results; (c) *in-situ* measurement results; and (d) comparison of test results. Reproduced with permission from Ref. [69], © IOP Publishing Ltd 2017.

compared the strip drawing test results with the *in-situ* measurement results and found that the COF measurement results of the two methods are basically the same. Shi et al. [45] used a standard tensile testing machine to build a simple high-temperature strip drawing testing device. Liewald et al. [72] improved the traditional strip drawing test by drilling micro-holes in the tool block, and studied the effect of CO_2 lubrication on sheet deep drawing friction. Han [73] used tool steel and frictionless rollers to clamp the metal strip, and pulled it to slide relative to tool steel. Based on strip drawing test, Kirkhorn et al. [74] developed the strip sliding friction test (Fig. 7(e)) by using a linear motor. The COF calculation in Refs. [73, 74] is shown in Eq. (2). Different from the actual forming process, strip drawing test does not consider the influence of tangential shrinkage of flange region.

$$\mu = \frac{T}{F_H} \tag{2}$$

3.2 Friction measurement in radius region

3.2.1 *BUT in die radius*

The BUT apparatus (Fig. 7(f)) is mainly used to simulate the friction behavior of die radius region. The force of the strip in BUT test is shown in Fig. 10(a), where T_1 is the tensile force, T_2 is the back tension, γ is the contact wrap angle, q is the average contact pressure, and R is the radius of roller [75]. From the perspective of force balance, Eq. (3) can be established.

$$\begin{cases} \mu q w R \mathrm{d}\gamma = \mathrm{d}T \\ q w R \mathrm{d}\gamma = T \sin\dfrac{\mathrm{d}\gamma}{2} + (T + \mathrm{d}T)\sin\dfrac{\mathrm{d}\gamma}{2} \end{cases} \tag{3}$$

where w is the width of metal strip.

From Eq. (1), Eq. (4) can be obtained.

$$\int_0^{\gamma} \mu \mathrm{d}\gamma = \int_{T_2}^{T_1} \frac{\mathrm{d}T}{T} \tag{4}$$

After integration, the μ is calculated as

$$\mu = \frac{1}{\gamma}\ln\frac{T_1}{T_2} \tag{5}$$

Considering the influence of R, the metal strip thickness t, and bending deformation force T_b, Eq. (5) can be rewritten as

$$\mu = \frac{1}{\gamma}\left(\frac{R + 0.5t}{R}\right)\ln\left(\frac{T_1 - T_b}{T_2}\right) \tag{6}$$

Han [73] and Sanchez [76] developed a BUT device with $\gamma = 90°$. Fratini et al. [77] used a lever to provide T_2 on the basis of Saha and Wilson [78], which greatly simplifies the structure of BUT device. Bay et al. [79, 80] designed a heatable BUT device with a temperature

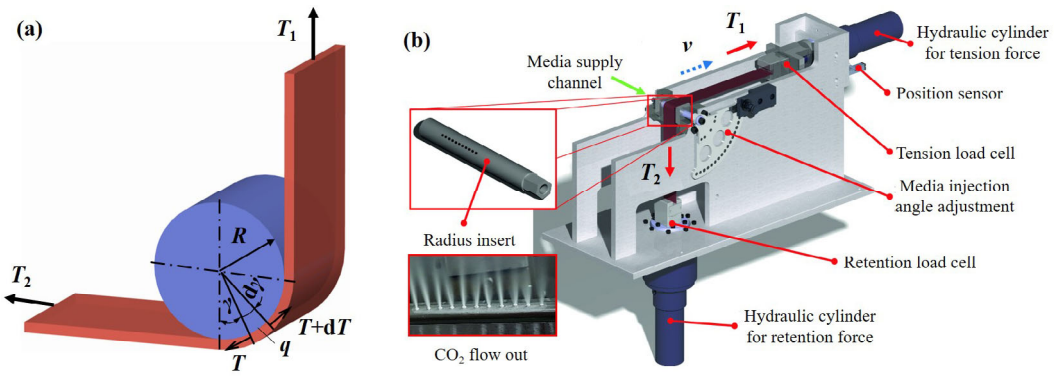

Fig. 10 (a) BUT radius force analysis; (b) BUT friction measurement device. Reproduced with permission from Ref. [82] for (b), © The Authors 2019.

control range from room temperature to 100 °C. Ramezani et al. [81] and Hwang and Chen [38] improved the traditional BUT device's inability to change the inclination angle, and studied the influence of different γ on COF. As shown in Fig. 10(b), Reichardt and Liewald [82] set up microchannels for the circulation of volatile media on die radius inserts, which expand the application range of BUT devices. Similar to the problems in strip drawing test, the BUT test does not consider the effect of sheet tangential shrinkage on friction.

3.2.2 *BUT in punch radius*

As shown in Fig. 7(g), BUT test in punch radius shares the same principle as BUT test in die radius. The difference is that one end of metal strip is fixed, and the other end slides around the roller surface under T_1. The COF calculation method is the same as that of Eq. (5). Trzepiecinski [83] used the BUT device to study the variation of punch radius friction with relative elongation of sheet. Since the traditional method needs to calculate the friction force indirectly by measuring the strain of the metal strip, Hao et al. [84] designed "L" and "U" shapes' friction test devices that can directly measure the friction force.

3.3 Compound friction test

As shown in Fig. 7(h), the compound friction test is a method for measuring the deep drawing friction that has emerged in recent years. It combines the strip drawing test with BUT test, and can measure the COF of flange region and radius region at the same time. The compound friction test device designed by Dilmec and Arap [85] is shown in Fig. 11. The metal strip is divided into two sections: One section is located in the flange friction region, the other section is located in the radius friction region, and the middle is connected by a force sensor. The test can only be carried out at a very low speed. Evin and Tomáš [86] could complete the friction measurement of flange region and radius region by stretching the metal strip at one time, which not only increases the stretching speed, but also gets closer to the actual forming conditions. But they are not compared with the strip drawing test results or the BUT test results, so the accuracy and reliability of the compound friction test need to be further verified.

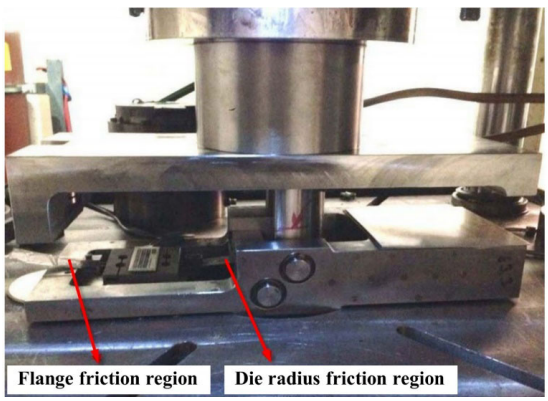

Fig. 11 Compound friction test device. Reproduced with permission from Ref. [85], © Springer-Verlag London 2015.

4 AADD friction model

Friction is one of the most important boundary conditions of AADD. However, the analysis in Section 2 shows that the COF in deep drawing is constantly changing due to many factors. In order to deeply study the internal mechanism of AADD friction,

it is necessary to establish a reasonable friction model to characterize the COF of AADD. Existing sheet metal deep drawing friction models can be roughly divided into two categories, i.e., the empirical friction model based on test results and the theoretical friction model based on theoretical derivation, as shown in Fig. 12. The empirical model can be subdivided into single-factor friction model and multi-factor coupled friction model. The theoretical model can be subdivided into macro-scale friction model, micro-scale friction model, and multi-scale friction model. Section 4 focuses on summarizing the friction models directly or indirectly related to AADD since 2000.

4.1 Empirical friction model

4.1.1 *Single-factor*

The single-factor friction model is a simple mathematical induction of the law of a single influencing factor. In 2020, based on the H13/AA6111 reciprocating friction test results under boundary lubrication conditions, Dou et al. [29] characterized the relationship between the v, the normal load F_{H}, and the μ, as shown in Eq. (7). Keum et al. [48] summarized the laws of five influencing factors through BUT test, and established a friction model considering v, sheet surface roughness and hardness, lubricating oil viscosity, and die radius.

$$\begin{cases} \mu = \dfrac{5.586}{v+15.52} + 0.005 \\ \mu = 0.138\left(\dfrac{15}{F_{\mathrm{H}}}\right)^{0.207} + 0.01 \end{cases} \tag{7}$$

4.1.2 *Multi-factor*

In order to study the interaction between different influencing factors under complex working conditions, it is necessary to establish a multi-factor coupled friction model. In 2019, Dou and Xia [87] built a friction model with comprehensive load and velocity effects. Klocke et al. [88] coupled the temperature in model, and further refined the friction model related to process parameters. To evaluate the effect of tool coating thickness $h(t)$ variation on the total friction $\mu(t)$ evolution, Zhou et al. [89] developed the interactive friction model (Eq. (8)) according to the results of the ball-on-disk friction test.

$$\mu(t) = \mu_{\mathrm{a}}(t) + \mu_{\mathrm{p}}(t)\exp\left[-(\kappa_1 h)^{\kappa_2}\right] \tag{8}$$

where $\mu_{\mathrm{a}}(t)$ is the initial friction, $\mu_{\mathrm{p}}(t)$ is the plowing friction when $h(t) = 0$, and κ_1 and κ_2 are the model parameters. In order to describe the evolution process of the contact interface from boundary lubrication to dry friction $\mu_{\mathrm{d}}(t)$, based on the Arrhenius equation, Yang et al. [44] established the interactive friction model (Eq. (9)) in 2021. The contribution of boundary friction $\mu_{\mathrm{l}}(t)$ and $\mu_{\mathrm{d}}(t)$ to $\mu(t)$ is characterized by the ratio between the non-lubricated area and the lubricated area ξ.

$$\mu(t) = (1-\xi)\mu_{\mathrm{l}}(1-\xi) + \xi\mu_{\mathrm{d}}(t) \tag{9}$$

The composition of the friction model proposed by Tamai et al. [90] is similar to that reported in Ref. [44], including a mixed lubrication part and a dry friction part. Hu et al. [60] developed a friction model related to aluminium transfer in pin-on-disk friction test. The model $\mu(t)$ can be decomposed into aluminium–CI

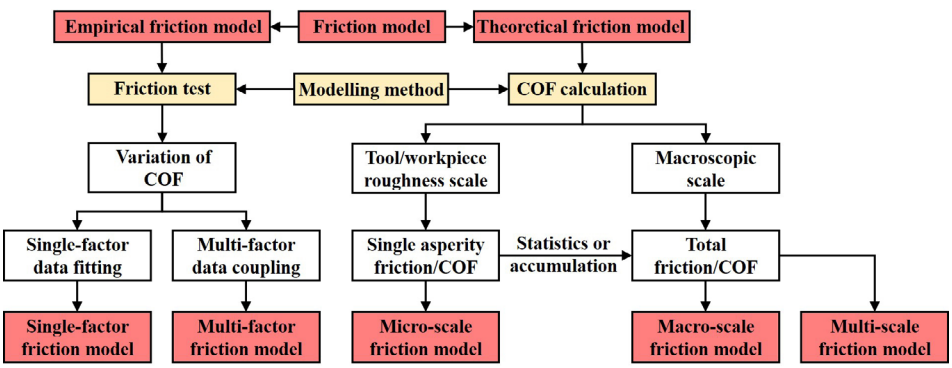

Fig. 12 Classification and construction methods of sheet metal deep drawing friction model.

contact friction $\mu_{\text{Al–CI}}$ and aluminium–aluminium contact friction $\mu_{\text{Al–Al}}$, where $\overline{f}(t)$ is the normalized transfer area.

$$\mu(t) = (1-\overline{f}(t))\mu_{\text{Al–CI}} + \overline{f}(t)\mu_{\text{Al–Al}} \tag{10}$$

Compared with that of the single-factor friction model, the friction behavior represented by the multi-factor friction model is closer to the real forming conditions.

4.2 Theoretical friction model

4.2.1 Macro-scale

The macro-scale friction model analyzes the friction mechanism of specific internal parameters and specific forming conditions. Based on Tabor's adhesive friction theory [91], Leu [92] established an extended friction model related to real contact area fraction α and strain hardening index n in three-dimensional (3D) stress element in 2009.

$$\mu = \frac{\alpha}{\sqrt{3}\left[\left(1-\alpha^2\right)^{1/2} + \alpha^{n/2}\right]} \tag{11}$$

where $\alpha = \tanh(3p/\sigma_{\text{u}})$, p is the normal pressure, and σ_{u} is the maximum tensile stress. It can be seen from Fig. 13 that the extended model improves the distortion of μ tending to infinity when the Tabor model is close to the adhesion state ($\alpha \approx 1$) [91]. Because the surface morphology of the die–sheet affects the real contact area A_{c}, Ramezani and Ripin [93] believed that $\alpha = erf\left(F_{\text{N}} / \sqrt{m_2}E'A_{\text{n}}\right)$ depends on the normal load F_{N} and root mean square rate of surface height m_2, where *erf* is a function, E' is the equivalent modulus, A_{n} is the nominal contact area, and the extended friction model is transformed into Eq. (12).

$$\mu = \frac{erf\left(F_{\text{N}} / \sqrt{m_2}E'A_{\text{n}}\right)}{\sqrt{3}\left[\left(1-\left(erf\left(F_{\text{N}} / \sqrt{m_2}E'A_{\text{n}}\right)\right)^2\right)^{1/2} + \left(erf\left(F_{\text{N}} / \sqrt{m_2}E'A_{\text{n}}\right)\right)^{n/2}\right]} \tag{12}$$

In order to capture the friction response between AA6111sheet and D2 tool steel, Gearing et al. [94] proposed the friction evolution equation related to p, $\overline{u}^{\text{s}}$, and hardening/softening function, as shown in Eq. (13).

$$\hat{s}(p,\overline{u}^{\text{s}}) = \begin{cases} \mu_1 p, & p \le p_{\text{cr}} \\ s^* \tanh\left\{\dfrac{\mu\left(p-p_{\text{cr}}\right)}{s^*}\right\} + \mu_1 p_{\text{cr}}, & p > p_{\text{cr}} \end{cases} \tag{13}$$

Among them, $\hat{s}$ is the slip resistance function, μ_1 is the conventional coefficient of Coulomb friction at low pressures, s^* is the interface sliding limit under high p, and p_{cr} is the critical pressure. Figure 14 shows that under solid lubricant boric acid, the friction model exhibits good agreement with the experimental results.

In addition, Wilson et al. [95] established a friction model from thick film and thin film to mixed and boundary lubrication states by judging the oil film thickness during deep drawing. In thick and thin

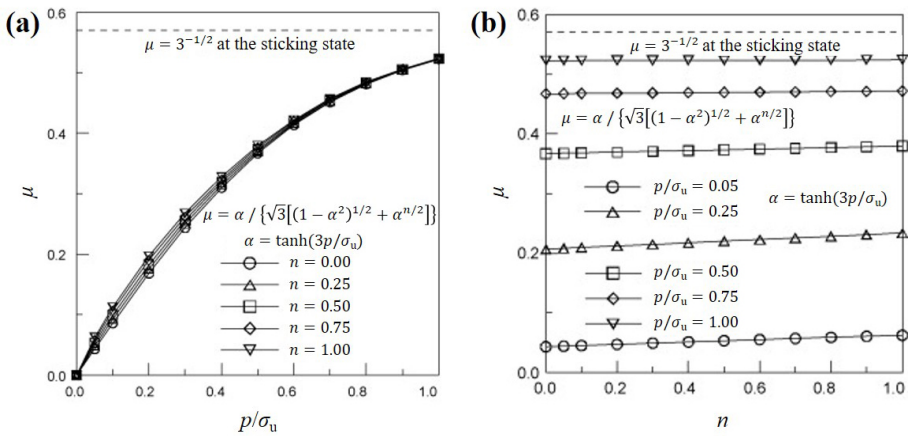

Fig. 13 Extended friction model based on Tabor model: (a) variation of μ with p/σ_{u} when n is different; (b) variation of μ with n when p/σ_{u} is different. Reproduced with permission from Ref. [92], © Elsevier B.V. 2008.

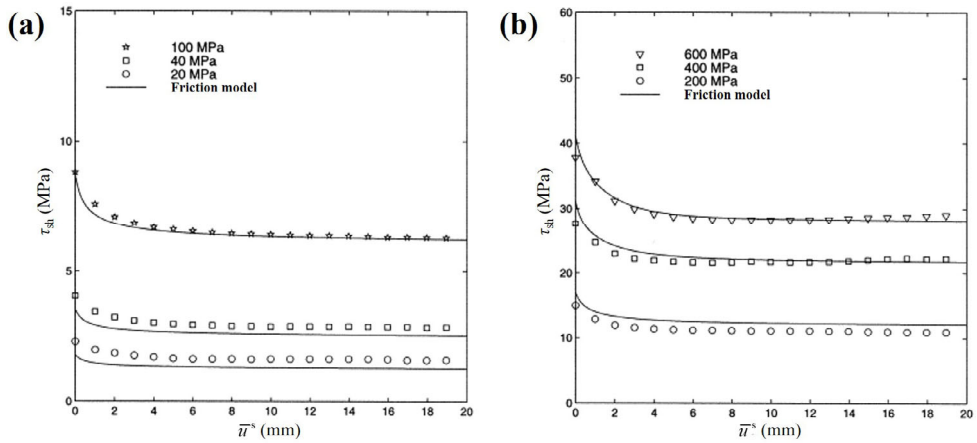

Fig. 14 Variation of interface shear stress τ_{sh} of AA6111/D2 with $\bar{u}^s$ and friction model fitting under boric acid lubricated under (a) low p; (b) high p. Reproduced with permission from Ref. [94], © Elsevier Science Ltd. 2001.

film state, the friction stress τ_f is only composed of hydrodynamic component τ_h. In the mixed lubrication state, there is solid surface contact, and τ_f adds adhesion component τ_a and plowing component τ_p, as shown in Eq. (14).

$$\tau_f = \tau_a\alpha + \tau_p\alpha + \tau_h(1-\alpha) \tag{14}$$

On the basis of this model, Darendeliler et al. [96] and Yang [97] introduced Wilson and Sheu's [61] semi-empirical equations about effective hardness, α, and dimensionless strain rate. The τ_f in the mixed and boundary lubrication states are modified. Başpınar and Akkök [98] analyzed the application scopes of Sojoudi and Khonsari [99] and Wilson et al. [95], and pointed out that a single friction model cannot cover the wide range of internal and external conditions. The combination of different models can not only improve the prediction accuracy, but also expand the scope of application. The macro-scale friction model establishes the link between specific forming parameters and overall friction effect, but ignores the effect of local topography changes and contact condition differences on deep drawing friction.

4.2.2 *Micro-scale*

The tool–workpiece (die–sheet) surface is nominally flat, but due to the presence of rough and uneven asperities at the micro level, contact only occurs at certain points, as shown in Fig. 15(a). The deep drawing friction is caused by shearing and plowing after tool asperities are pressed into the workpiece surface. The micro-scale friction calculation is inseparable from the force of tool asperity and the

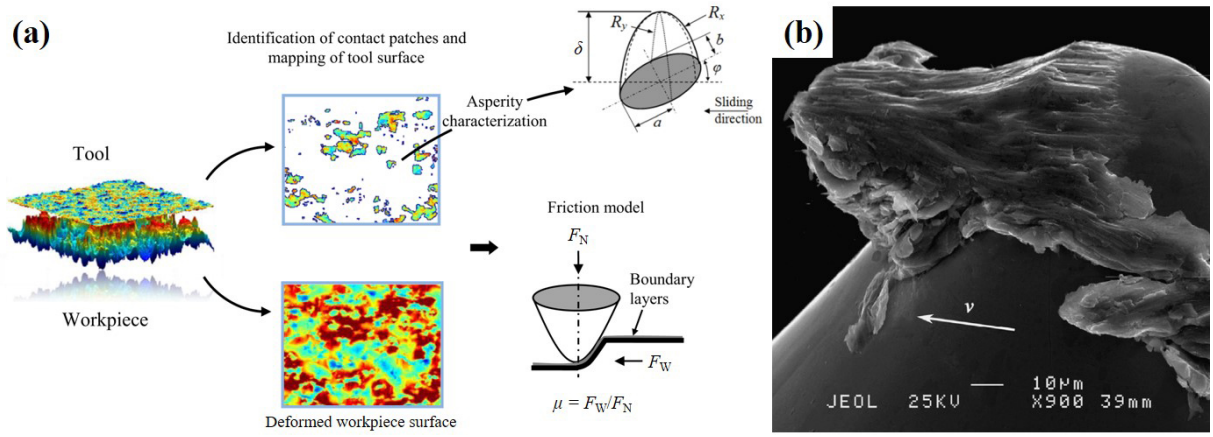

Fig. 15 (a) Tool–workpiece contact during deep drawing process; (b) aluminium transfer of tool pin tip. Note: b is the nominal contact width. Reproduced with permission from Ref. [101] for (a), © Elsevier B.V. 2014; Ref. [102] for (b), © Elsevier B.V. 2013.

deformation of workpiece asperity. As the contact load increases, the workpiece asperity needs to undergo a long elastoplastic transformation from elastic deformation to full plastic flow. A single elastic or plastic contact model is difficult to characterize the complex contact situation of asperity in deep drawing process. Therefore, Zhao et al. [100] proposed a contact model that includes the entire process of elastoplastic deformation of workpiece asperity in 2000. Based on this model, Karupannasamy et al. [101] further established a contact model for calculating the normal loading force of a single tool asperity in 2014. Because aluminium alloy sheets are prone to aluminium transfer during deep drawing, as shown in Fig. 15(b), de Rooij et al. [102] studied the geometrical evolution of tool asperity and established a single asperity scale material transfer model.

On the micro-scale level, the interface asperities are irregularly arranged and have different shapes. It is necessary to appropriately simplify the geometry of asperity to calculate the rigid tool asperity force and the soft workpiece asperity deformation. At present, the simplified asperity geometry used for micro-scale friction calculation is shown in Fig. 16. Two-dimensional (2D) geometry includes wedge and cylinder, and 3D geometry includes sphere, cone, and elliptical paraboloid. Mishra et al. [103–105] established a single spherical asperity plowing model, analyzed the effects of normal load, asperity size, and interface shear strength on $\mu_p(t)$, and predicted the COF and plowing depth of a single asperity sliding against the substrate. Compared with other geometric shapes, elliptical paraboloids can control and describe asperity geometric shapes more realistically. In recent years, the micro-scale friction model based on this has been developed rapidly [106–109]. According to the work done by Bowden et al. [110], Mishra et al. [106] calculated the frictional force vector $\boldsymbol{F}$ acting on a single elliptical parabolic asperity in 2019. The expression is similar to that of the macroscopic friction model (Eq. (14)). Equation (15) is composed of the plowing part $p_{pl}A_c\hat{\boldsymbol{n}}$ and adhesive part $\tau_{sh}A_c\hat{\boldsymbol{t}}$.

$$\boldsymbol{F} = p_{pl}A_c\hat{\boldsymbol{n}} + \tau_{sh}A_c\hat{\boldsymbol{t}} \tag{15}$$

Among them, p_{pl} is the real contact pressure, A_c is the real contact area, τ_{sh} is the interface shear stress, $\hat{\boldsymbol{n}}$ is the unit normal vector, and $\hat{\boldsymbol{t}}$ is the unit tangential vector. This model studies the variation of frictional force with size, ellipticity, and orientation angle of asperity, but ignores the influence of material accumulation at the front end of asperity, as shown in Fig. 17. To make up for this shortcoming, Shisode et al. [107] improved the calculation accuracy of model by introducing a stacking factor in 2021. Challen and Oxley [111, 112] conducted a slip line field analysis on the deformation of soft flat materials under hard wedge-shaped asperity. The cutting friction coefficient $\mu_{cutting}$, plowing friction coefficient $\mu_{plowing}$, and wear friction coefficient μ_{wear} are described as a function of attack angle θ of wedge-shaped asperity and the shear coefficient f_c, as shown in Eqs. (16)–(18).

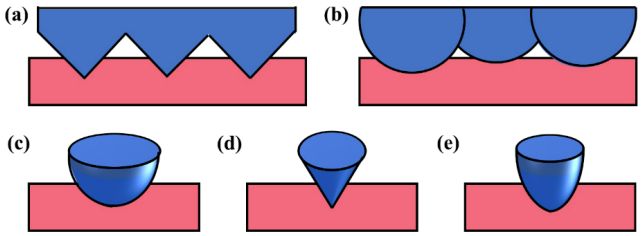

Fig. 16 Simplified geometry of asperity: (a) wedge; (b) cylinder; (c) sphere; (d) cone; and (e) elliptical paraboloid.

$$\mu_{cutting} = \tan\left(\theta - \frac{1}{4}\pi + \frac{1}{2}\arccos f_c\right) \tag{16}$$

$$\mu_{plowing} = \frac{A_1\sin\theta + \cos(\arccos(f_c - \theta))}{A_1\cos\theta + \sin(\arccos(f_c - \theta))} \tag{17}$$

$$\mu_{wear} = \frac{\left(1 - 2\sin A_2 + \sqrt{1 - f_c^2}\right)\sin\theta + f_c\cos\theta}{\left(1 - 2\sin A_2 + \sqrt{1 - f_c^2}\right)\cos\theta + f_c\sin\theta} \tag{18}$$

where

$$\begin{cases} A_1 = 1 + \dfrac{1}{2}\pi + \arccos f_c - 2\theta - 2\arcsin\left(\dfrac{\sin\theta}{\sqrt{1 - f_c}}\right) \\ A_2 = 1 - \dfrac{1}{4}\pi - \dfrac{1}{2}\arccos f_c + \arcsin\left(\dfrac{\sin\theta}{\sqrt{1 - f_c}}\right) \end{cases} \tag{19}$$

Hol et al. [108, 113] and Karupannasamy et al. [114] calculated the μ of a single cylindrical or elliptical parabolic asperity sliding across the workpiece surface during the deep drawing process on the basis of

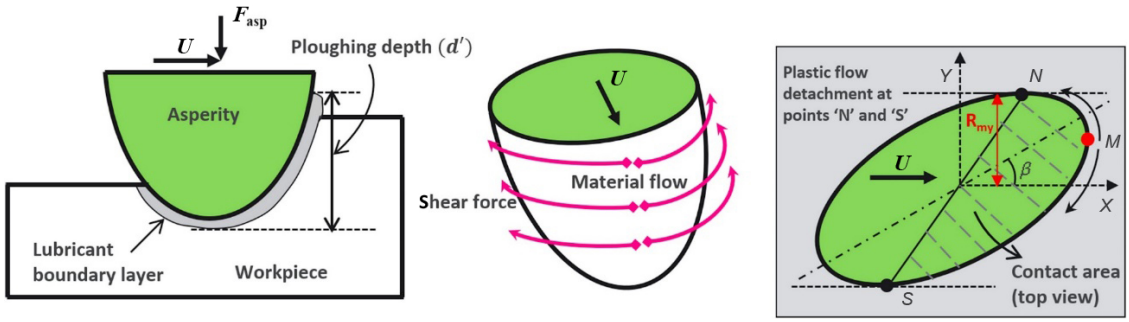

Fig. 17 Schematic diagram of elliptical paraboloid asperity plowing. Reproduced with permission from Ref. [107], © The Authors 2020.

Challen and Oxley [111, 112]. The micro-scale contact and friction model studies the force deformation process and friction mechanism of the die–sheet asperity, and explains the interface interaction at the micro level, which helps to analyze the friction response changes caused by local contact differences.

4.2.3 *Multi-scale*

The micro-scale friction model can more realistically and accurately reflect the friction characteristics of deep drawing. However, the model is too cumbersome to be applied to the calculation of large-scale sheet metal forming. For this reason, it is necessary to adopt appropriate methods to expand the model from micro-scale to macro-scale. Multi-scale friction model has emerged. The evolution processes of sheet surface morphology during deep drawing are shown in Fig. 18. It can be seen that under normal load and sliding friction, the flattening of the sheet asperities leads to an increase in the macroscopic A_c. At present, the method of establishing multi-scale friction model is as follows: (1) The process parameters and material properties are input; (2) the flattening model of sheet asperities with the normal load is established; (3) the sliding flattening model of sheet asperities is established; (4) the indentation depth of tool asperities on the sheet surface is calculated; (5) the friction force of single asperity $F_{friction}$ is calculated; and (6) the macroscopic COF is calculated.

In deep drawing process, constructing a cross-scale contact model to solve the A_c is the basis for calculating the multi-scale friction model. The cross-scale contact model for predicting the flattening behavior of rough surfaces mostly continues the pioneering work of

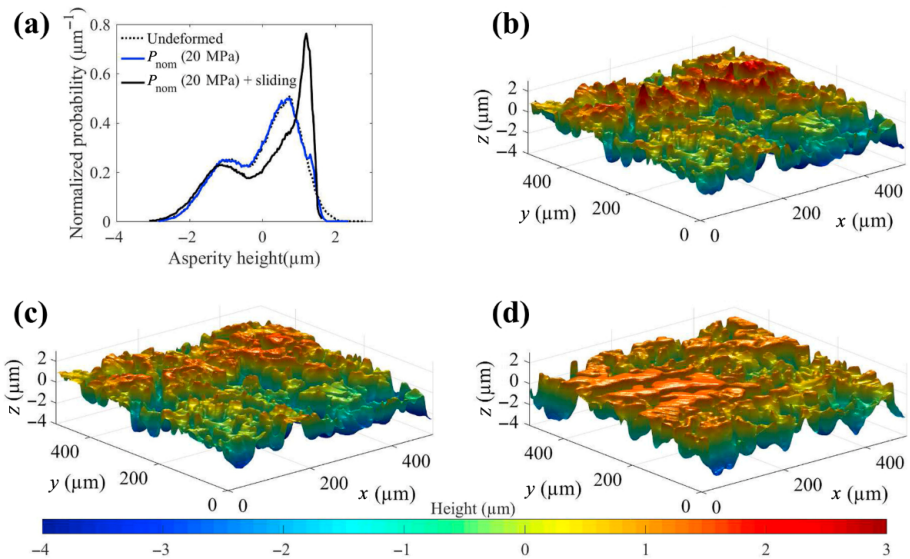

Fig. 18 Evolution processes of sheet surface morphology: (a) deformed and undeformed surface height distribution $\phi(z)$; (b) initial surface; (c) normal loading deformation; and (d) normal loading+sliding deformation. Reproduced with permission from Ref. [107], © The Authors 2020.

Greenwood and Williamson (GW model) [115]. However, the GW model is based on Hertzian elastic contact theory. It cannot calculate the plastic deformation of asperities. Pullen and Williamson [116] assumed that the asperities on non-contact surface rise uniformly, and the problem was solved by volume conservation and energy conservation. Inspired by Pullen and Williamson [116], Westeneng [117] derived a plastic contact model that replaces the peak height distribution with the $\phi(z)$ in 2001. Since the Westeneng model [117] can describe asperity deformation of any shape and is closer to the real forming conditions, it has been developed rapidly in the past ten years [107, 108, 113, 114, 118–122]. The contact between smooth tool surface and rough sheet surface is shown in Fig. 19(a). The sheet surface in the model is identified by bars of equal width. Given the surface height distribution $\phi_{\mathrm{W}}(z)$ and p, the energy conservation and volume conservation equations (Eqs. (20) and (21), respectively) are combined using statistical methods to obtain the uniform rising of non-contact surface U_{L} and the mean plane of rough sheet surface d_{L}. Then the α can be calculated by Eq. (22).

$$p = \frac{B}{A_{\mathrm{n}}}\left(\frac{\xi}{\omega} + \eta\frac{\chi}{\omega}\right) + \frac{S}{A_{\mathrm{n}}}\frac{\psi}{\omega} \tag{20}$$

$$U_{\mathrm{L}}(1-\alpha) = \int_{d_{\mathrm{L}}-U_{\mathrm{L}}}^{\infty}(z-d_{\mathrm{L}})\phi_{\mathrm{W}}(z)\mathrm{d}z \tag{21}$$

$$\alpha = \int_{d_{\mathrm{L}}-U_{\mathrm{L}}}^{\infty}\phi_{\mathrm{W}}(z)\mathrm{d}z \tag{22}$$

Among them, B = 2.8 representing the hardness factor, $S = 1/\sqrt{3}$ following the Von Mises yield criterion, ω is the indentation coefficient, ζ is the energy required to flatten the contact bar, χ is the energy required to lift the non-contact bar, ψ is the energy required to shear bar with relative motion, η is the roughness durability parameter, and z is the surface height. Furthermore, the interface sliding test shows that sliding contact induces junction growth, which promotes the A_{c} of die–aluminium alloy sheet interface to further increase [123–125]. This is because the increase in the subsurface volume strain of sheet material leads to a substantial decrease in hardness of asperities. The α needs to be combined with the influence of this effect [61, 126, 127].

After the A_{c} is obtained through the cross-scale contact model, the multi-scale friction model is used to realize the calculation of deep drawing friction from micro-scale to macro-scale. At present, there are two methods for establishing multi-scale friction models: direct accumulation and statistical transformation [107, 108, 113, 114, 118–122]. The direct

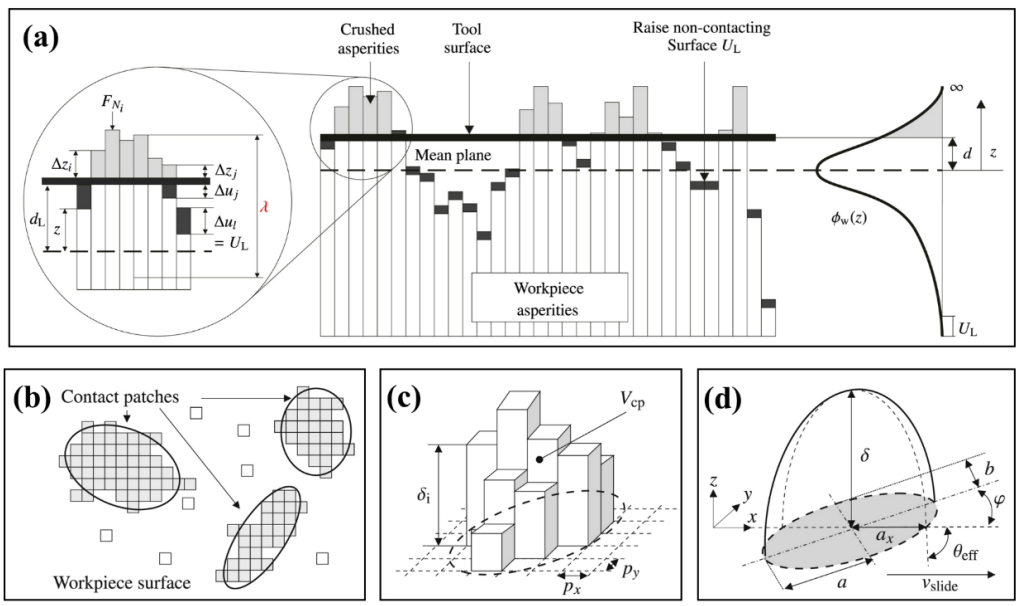

Fig. 19 Contact surface recognition and simplification: (a) smooth tool surface in contact with rough sheet surface; (b) contact patches; (c) contact volume; and (d) asperity geometry. Note: δ is the distance between sheet surface and average plane of die asperities. Reproduced with permission from Ref. [108], © Elsevier Ltd. 2014.

accumulation method is based on the image recognition technology, as shown in Figs. 19(b)–19(d), fitting all elliptical parabolic asperities k on die surface, and calculating the friction force of each asperity f in turn according to Eqs. (15)–(18). The cumulative f is divided by normal load F_N to calculate macro-scale μ.

$$\mu = \frac{\sum_{i=1}^{k}(f)_i}{F_N} \tag{23}$$

The statistical transformation method is based on the distribution function of die surface asperities $\phi_t(s)$, die surface asperity density ρ_t, nominal contact length l_{nom}, nominal contact width b, distance between sheet surface and average plane of die asperities δ, and the maximum height of die asperities G_{max}. Using statistical methods, the $F_{W_{asp}}(\theta)$ is extended to macro-scale.

$$\mu = \frac{F_W}{F_N} = \frac{\alpha l_{nom} b \sqrt{\rho_t} \int_{\delta}^{G_{max}} F_{W_{asp}}(\theta)\phi_t(s)\mathrm{d}s}{F_N} \tag{24}$$

Compared with single-scale friction model, multi-scale model fully characterizes the friction evolution process of interface from micro-scale to macro-scale. Solving the shortcomings that micro-scale model is difficult to calculate on large-scale and macro-scale model cannot distinguish local differences. However, multi-scale model is still based on a lot of simplifications and assumptions. And there is a big gap between multi-scale model and actual friction contact. How to improve the calculation efficiency and calculation accuracy of model under the condition which is as close to the engineering practice as possible. It has become an urgent problem to be solved in the research of multi-scale friction model.

5 AADD friction simulation

As the demand for aluminium alloy parts continues to increase, simulation must be used for quality control and problem analysis in the early stage of product development and later production. In simulation of deep drawing process, the COF of the entire area is usually assumed to be constant according to Coulomb's law, which is significantly different from the real forming conditions of AADD, causing serious calculation errors. Currently, there are two main pathways to solve this problem: constant COF simulation based on COF sub-domain setting and variable COF simulation based on the development of friction model. The two methods have their own advantages. The constant COF simulation contributes to inversely solving the tribological conditions favorable to AADD. The variable COF simulation contributes to improving the prediction accuracy of AADD performance. Section 5 clarifies the characteristics and applications of the two simulation methods in turn.

5.1 Constant COF simulation

The constant COF simulation is easy to perform and can be realized by using commercial software such as ABAQUS, ANSYS, LS-DYNA, DEFORM, and DYNAFORM. This method mainly includes the following four steps: (1) Different COFs in different contact areas are set; (2) the forming performance metrics are set to be tested, such as thinning, wrinkling, and cracking; (3) the simulation results are compared, analyzing the influence of COF on forming performance metrics; and (4) the best forming tribological conditions are inversely solved. For this reason, Bouchaâla et al. [18, 128] set up different COF in three contact areas of sheet–punch, sheet–holder, and sheet–die, taking the wall thickness reduction rate as test metrics, using the orthogonal test studied the effect of COF on the wall thickness distribution of two aluminium–lithium alloys (AA2198 and AA2090), and determined the COF combination with the smallest wall thickness reduction. In order to improve the quality of AA6182 deep drawing, Shivpuri and Zhang [129] studied the friction distribution optimization design to reduce the risk of wrinkling and cracking in 2009. The division of deep drawing contact area is more detailed, as shown in Fig. 20(a). Based on constant COF simulation, the optimal design of friction distribution is obtained. In addition, constant COF simulation can also be used to study the influence of friction on AADD forming limit, wall thickness uniformity, failure mode, and failure location [19, 22]. Although constant COF simulation has the above applications and advantages, it does not consider the dynamic response of COF during deep drawing

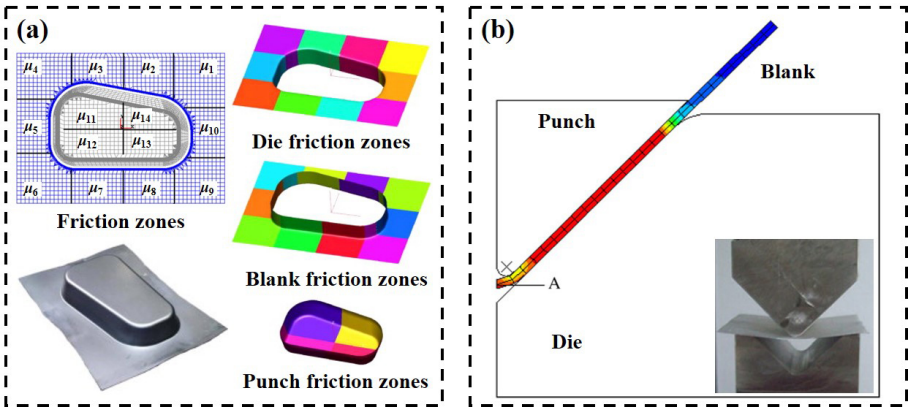

Fig. 20 (a) Friction distribution optimization design to reduce the risk of wrinkling and cracking; (b) stress distribution of V-bending simulation of aluminium alloy sheet. Reproduced with permission from Ref. [129] for (a), © Elsevier Ltd. 2008; Ref. [93] for (b), © Springer-Verlag London Limited 2010.

process, and the simulation results cannot be directly applied to the engineering practice.

5.2 Variable COF simulation

In variable COF simulation, the COF changes in real time, and it is based on the empirical friction model and theoretical friction model, as shown in Section 4. Compared with the constant COF simulation, the simple empirical friction model can be realized through custom settings in commercial software, while the complex theoretical friction model requires the user to write a special program. The empirical friction model that fits the influence of pressure and speed can be input into software, which can directly simulate the variable COF of AADD, such as AA6016, AA6111, and AA5052. Comparing the measurement results of the thickness distribution and springback obtained by simulation and experiment, variable COF simulation results improve the overall prediction accuracy of deep drawing parts [29, 87, 130]. Zhou et al. [89] proposed a Knowledge Based Cloud Finite Element (KBC-FE) simulation technique. By combining the interactive friction model established by Eq. (8) with the conventional finite element simulation, the life prediction of coated tool in multi-cycle loading AA5754 can be realized. The macro-scale friction model is established based on Eqs. (12)–(14), which integrates the influence of internal material parameters and external forming conditions. Integrating the friction model into the finite element program can simulate variable COFs from $\mu_d(t)$ to different lubrication states [93, 94, 96]. The stress distribution of AA6061 sheet after V-bending in dry friction state is shown in Fig. 20(b). Based on multi-scale friction model established by steel, Wiklund et al. [131, 132] extended it to AA6016 deep drawing simulation, demonstrating the application potential of multi-scale friction model in AADD variable COF simulation.

In the past decade, with the help of multi-scale friction models that systematically consider the state from boundary friction to mixed lubrication, Hol et al. [108, 113, 118], Shisode et al. [107, 121, 122], and Karupannasamy et al. [114] used an in-house software Dieka developed by University of Twente to conduct deep drawing simulation on several typical parts, such as cross-die, top-hat, and cup, and verified the accuracy of multi-scale friction models by comparing with the experimental results. These models provide theoretical support for the large-scale application of TriboForm software. TriboForm can describe the COF dependence of contact pressure, v, plastic strain, and temperature under the given combination of material, surface topography, coating, lubricant type, and amount parameters, and creates a friction model that fits the actual production for the tribological system. References [39, 133, 134] have shown that the TriboForm friction model is applied to deep drawing simulation of AA5182, AA6016, AL6-OUT, etc., which improves the prediction accuracy of F_D, draw-in, major strain, thickness, and springback. This demonstrates its effectiveness in AADD variable COF simulation. Since 2016, there is an extensive collaboration on friction modelling between Volvo cars [135–142], Mercedes-Benz cars [133, 143], Ford cars [144],

Renault cars [145], Opel cars [5, 146], and TriboForm engineering. The involved automotive panels are Volvo's inner door, front door ringframe, A-pillar reinforcement panel, and fender, Mercedes-Benz's door-outer and front fender, Ford's hood inner panel, Renault's trunk lid inner part, and Opel's spare wheel well. The forming simulations and experimental measurements of Volvo XC90 inner door (Fig. 21) indicate that the simulation results based on the TriboForm friction model are in good agreement with the experimental measurement results compared with those of the constant COF simulations [137]. This is also confirmed by the simulation and experimental results of Ford Transit aluminium hood inner panel (Fig. 22(a)) and Mercedes-Benz aluminium front feeder (Figs. 22(b) and 22(c)) [133, 144]. However, in 2018, van Beeck et al. [147] pointed out that the prediction accuracy under deep drawing and tensile loading conditions is less because the TriboForm friction model does not consider complex deformation modes. In 2022, Zabala et al. [130] developed a new TriboZone friction model based on the TriboForm friction model. This model can assign TriboForm friction models to different regions of the die to evaluate the influence of local roughness on the deep drawing of AA6016 fender, as shown in Fig. 23. The results showed that TriboZone and TriboForm friction models predict similar results, with local roughness having a moderate impact on AADD. The variable COF simulation developed on the basis of friction model can more realistically reflect the whole process of AADD forming, which contributes to shortening the development cycle and reduce the production cost.

6 AADD friction control

During the AADD process, due to its adhesion tendency, it is easy to form aluminium "accumulation" on die surface, which deteriorates the tribological conditions

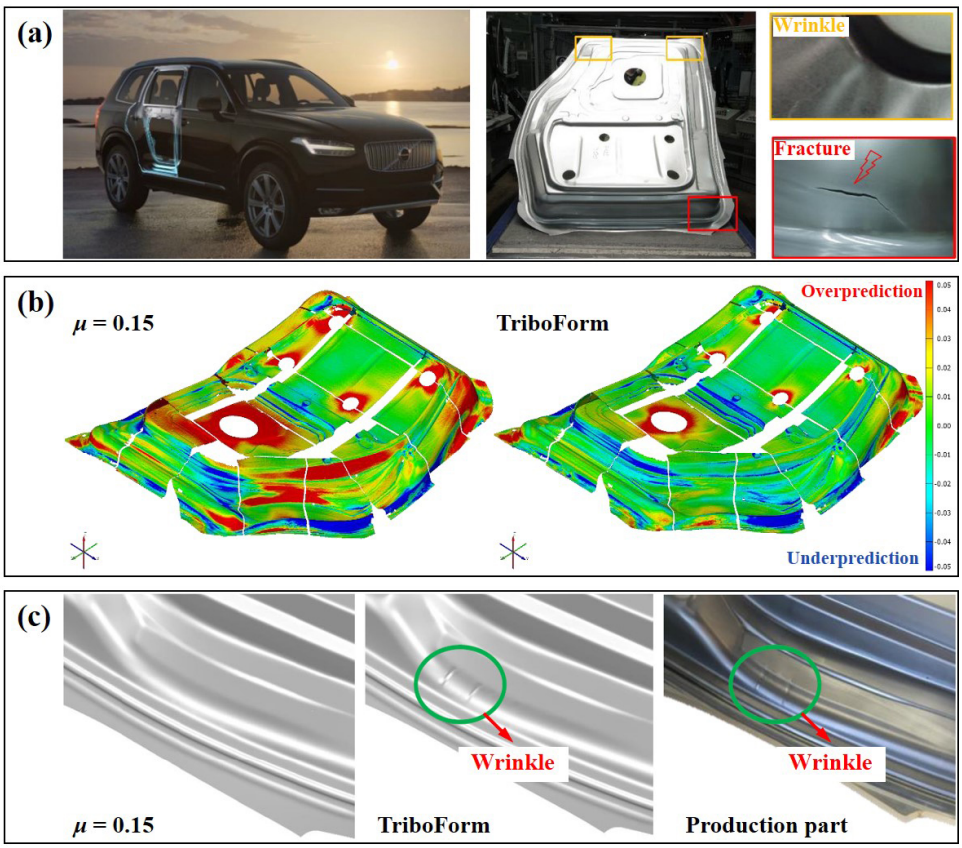

Fig. 21 Forming simulations and experimental measurements of Volvo XC90 inner door: (a) wrinkle and fracture of inner door in production; (b) major strain difference between simulations and experimental measurements; and (c) part shape difference between simulations and experimental measurements. Reproduced with permission from Ref. [137], © IOP Publishing Ltd 2016.

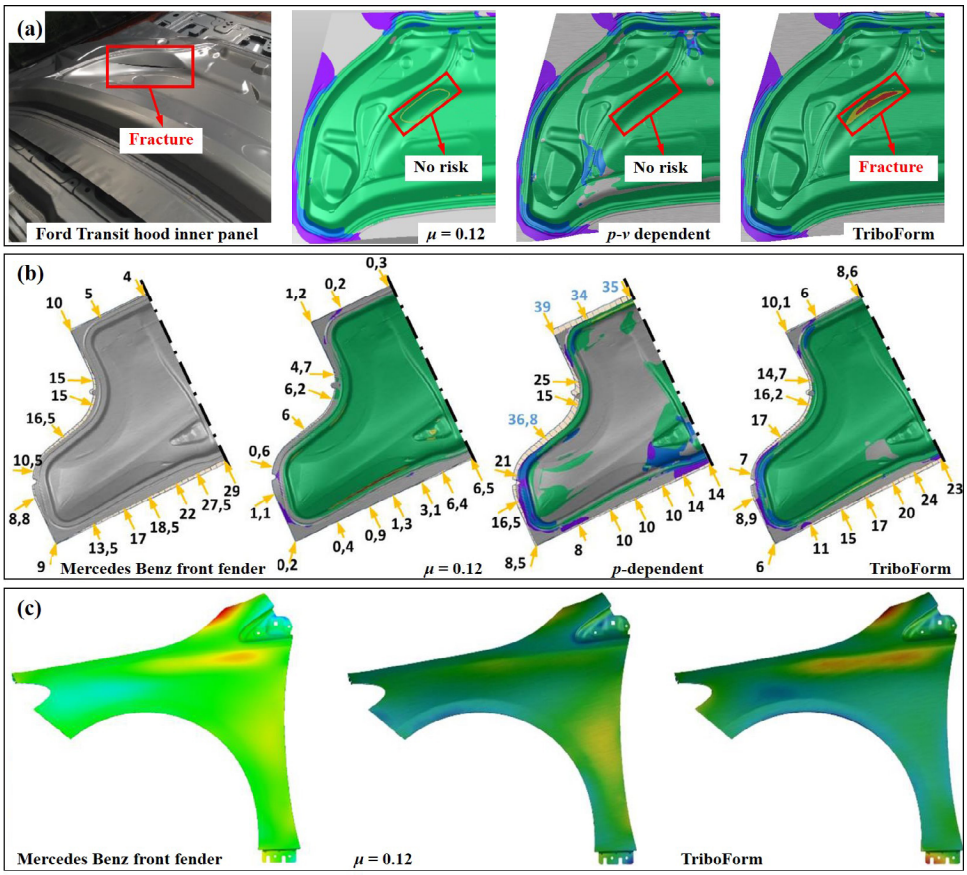

Fig. 22 Simulation and experimental results of AADD: (a) deep drawing results of Ford Transit aluminium hood inner panel; (b) draw-in and (c) springback results of Mercedes-Benz aluminium front fender. Reproduced with permission from Ref. [144] for (a), © IOP Publishing Ltd 2020; Ref. [133] for (b, c), © IOP Publishing Ltd 2019.

of AADD. Therefore, in traditional deep drawing process, lubricating oil is used to separate die and sheet to reduce friction and avoid wear. However, most of the industrial lubricants contain harmful ingredients, and the disposal of lubricant waste has caused serious environmental problems. The cleaning before each operation also greatly reduces the production efficiency. In the context of global advocacy of environmental protection, effective utilization of resources, and sustainable development, the development of lubrication-free method suitable for AADD has become an urgent problem to be solved. Section 6 reviews the application of solid lubrication, surface texture, coating modification, and composite treatment methods in controlling AADD friction.

Solid lubrication overcomes the inherent shortcomings that lubricating oil pollutes the environment, and die and part need to be cleaned after deep drawing. It can replace lubricating oil to be used under severe conditions such as high temperatures, low temperatures, vacuum, and heavy loads. Solid lubricants can be divided into soft metals, metal compounds, inorganic substances, and organic substances according to the types of raw materials. Typical materials used as solid lubricants include layered materials such as graphite and molybdenum disulfide, soft metals such as lead and silver, and polymer materials such as polytetrafluoroethylene and nylon. Although solid lubricants have great potential to replace lubricating oils, there are few results in studying their control of AADD friction. In 2017, only Ghiotti et al. [148] studied the effect of three different solid lubricants on the deep drawing friction behavior of AA6016 sheets under high-temperature conditions of 300–400 °C. The prepared solid lubricants include Pulve BND 60A based on boron nitride, Pulve D18A based on molybdenum disulfide, and Bonderite L-GP Aquadag based on graphite. The surface topographies and

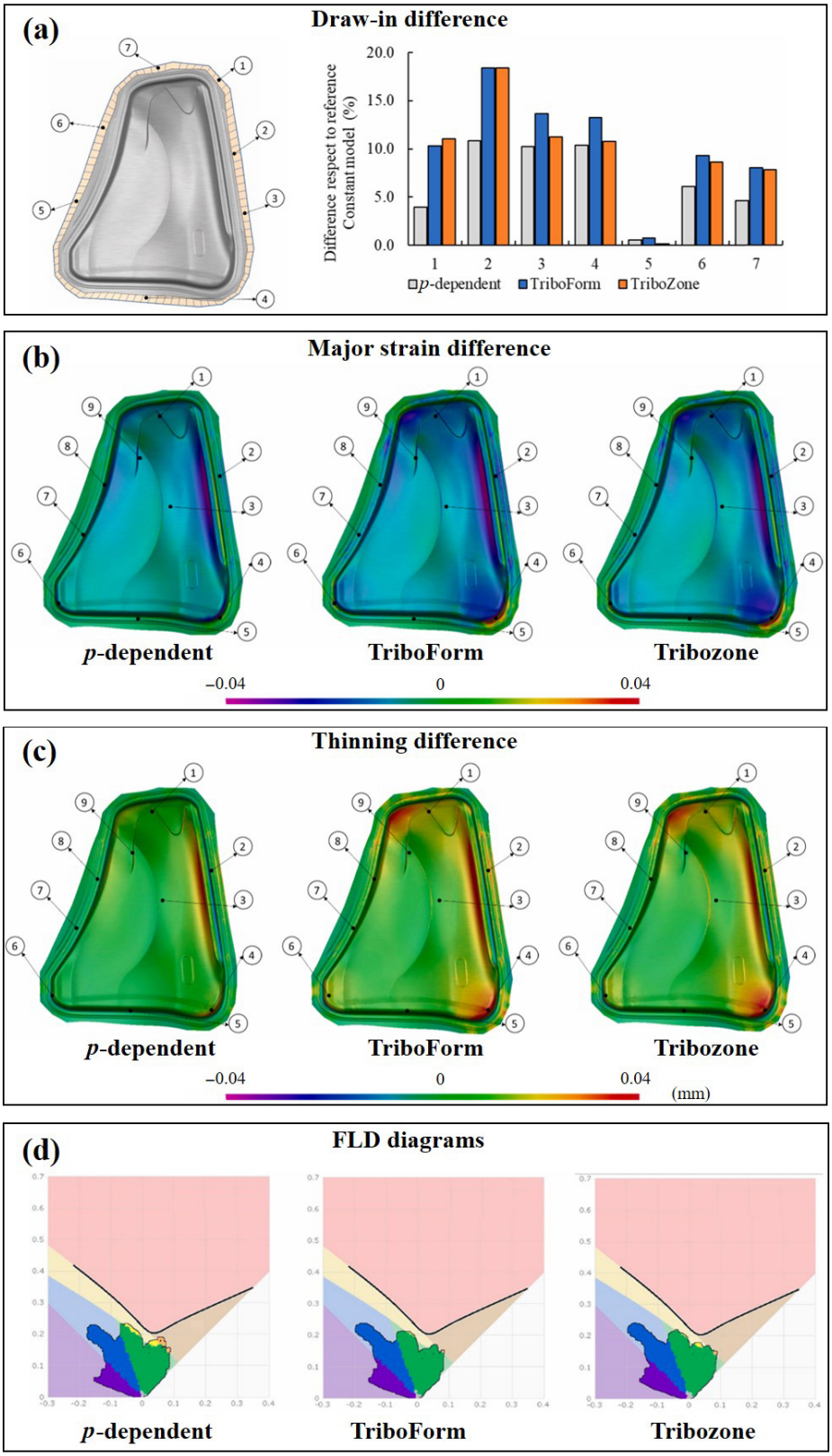

Fig. 23 Simulation results of *p*-dependent, TriboForm, and TriboZone friction models relative to constant friction models for aluminium fender deep drawing: (a) draw-in difference; (b) major strain difference; (c) thinning difference; and (d) forming limit diagram (FLD) diagrams. Reproduced with permission from Ref. [130], © The Author(s) 2021.

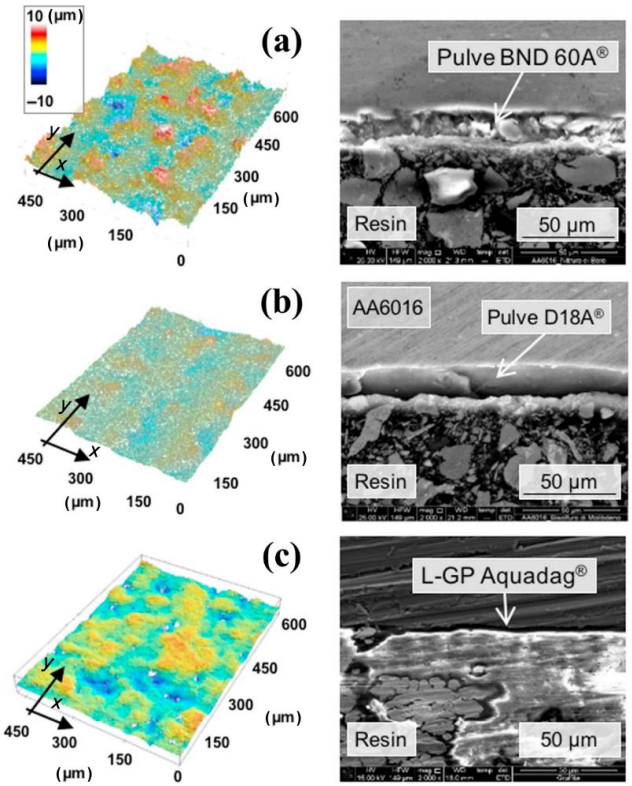

Fig. 24 3D surface topographies and SEM cross-sections of AA6016 sheet in deposited solid lubricants: (a) Pulve BND 60A; (b) Pulve D18A; and (c) Bonderite L-GP Aquadag. Reproduced with permission from Ref. [148], © Elsevier B.V. 2017.

scanning electron microscopy (SEM) cross-sections of sheet are shown in Fig. 24. High-temperature friction tests showed that the graphite lubricant has the best performance and can maintain a low COF over a long stroke range, while boron nitride and molybdenum disulfide lubricants are easily peeled off the matrix, which is not suitable for high-temperature forming of AA6016 sheets. The applicability of solid lubrication in different aluminium alloys and deep drawing process remains to be further explored.

Surface texture design is an important approach to controlling AADD friction. On the one hand, the textured cavity can capture aluminium chips to avoid scratches. On the other hand, it can store lubricants to reduce friction. According to different preparation methods, it can be divided into laser surface texturing (LST), discharge surface texture, hammered surface texture, milled surface texture, and photochemical surface texture. Commonly used patterns are circle, ellipse, triangle, wedge, square, and channel; the main parameters include size, depth, spacing, and density. References [54, 149–152] have confirmed the positive effect of die or sheet surface texture in reducing AADD friction. However, some researchers have challenged this view. Flegler et al. [153] and Hu and Hu [154] believed that the preparation of texture on die or sheet surface is not only difficult to alleviate adhesion between aluminium and die, but also increases the interface COF of AADD. In addition to the controversial friction control effect, the texture cannot maintain structural stability during long-term use due to wear and aluminium adhesion, and the friction control function is greatly restricted. The proper resolution of the above issues is related to whether surface texture can be applied to mass production of AADD.

It is well-known that coating can be used as a separation layer between die and sheet, so that die can adapt to complex and time-varying tribological conditions. And it can extend the service life of die while improving the forming quality of part. In the AADD process, due to excellent wear resistance and lubricating properties of carbon-based coating, it has received a great deal of attention from researchers [50, 52, 53, 62, 71, 155–158]. Hydrogenated amorphous carbon (a-C:H)-based coatings, also known as diamond-like (DLC) carbon coatings, are carbon-based coatings commonly used by AADD. Due to its unique net-like carbon structure, the coating combines the advantages of diamond and graphite, with high hardness and wear resistance. The application of a-C:H coating significantly reduces the COF of AADD and the adhesion transfer of aluminium alloy material in a dry forming process, and realizes the stable production of high-quality aluminium alloy parts without lubricating oil. However, high-temperature friction tests show that the friction properties of a-C:H coatings are temperature-dependent. The anti-friction effect decreases with the increase of temperature. Tetrahedral amorphous carbon (ta-C)-based coating is another commonly used carbon-based coating with similar functional effects to a-C:H coatings. The difference is that when the ta-C coating is in contact, a graphite-like transfer layer is formed at the interface. As a result, the lubricating performance of ta-C coating is better than that of a-C:H coating, and the anti-wear effect is better. On the basis of ordinary carbon-based coatings, the developed tungsten-doped carbon-based

coatings can further reduce the adhesion of AADD [71]. In recent years, in order to minimize the adhesion and friction of AADD, composite coatings with soft lubricating phase embedded in hard coatings have gradually emerged, such as micro-arc oxidation/graphite nanocomposite coatings, self-lubricating NC/NiBN, and NC/WC:C composite coating [159, 160]. In addition, the applicability of some conventional coatings has also been verified, and the results show that except for Cr coatings, TiCN, CrN, and TiN coatings are not suitable for AADD [155, 161]. Compared with solid lubrication, coating modification is a universal surface treatment method. The application research on AADD is more comprehensive and systematic, and its effectiveness has also been confirmed by production practice.

The composite treatment method refers to the friction control method of any combination of three lubrication-free methods of solid lubrication, surface texture, and coating modification. The existing AADD composite treatment method includes surface texture + solid lubrication and surface texture + coating modification. In 2019, Maldonado-Cortés et al. [162] discussed the synergistic effect of microchannel texture and TiO_2 nanoparticles (NPs). The microchannel textures of two orientations on die surface are shown in Fig. 25(a). The results of different combinations of ring-on-block test are shown in Fig. 25(b). It can be seen from Fig. 25 that compared with the die surface without any treatment, microchannel texture or TiO_2 NPs can greatly reduce the COF. Among them, the microchannel texture parallel to the sliding direction has the best friction reducing effect, and the synergistic effect of microchannel texture and TiO_2 NPs will increase or decrease the COF. Tenner et al. [163] studied the friction properties of AADD with rectangular or linear textured ta-C coatings, and the results showed that their friction increasing effect was significant. Contrary to the expected results, linear textured ta-C coatings not only does not reduce friction, but also the COF is higher than that of rectangular texture ta-C coating. Inspired by hydrophobic plants, Tillmann et al. [164] proposed five biomimetic textures of deposited CrAlN coatings, as shown in Fig. 26, which can provide references for AADD friction control. Low friction is not always beneficial to AADD. For example, the punch radius region requires a high COF to avoid cracking. Therefore, the development of a surface composite treatment method that controls local friction characteristics is of great interest to obtain high-quality AADD parts.

7 Conclusions and perspectives

In conclusion, we first analyzed the important role of friction in AADD and its influencing factors. The main regions to control friction are flange region, die radius region, and punch radius region. The influencing factors include process parameters, lubrication conditions, surface characteristics, and material properties. Then, according to the divided main friction regions, friction measurement methods for

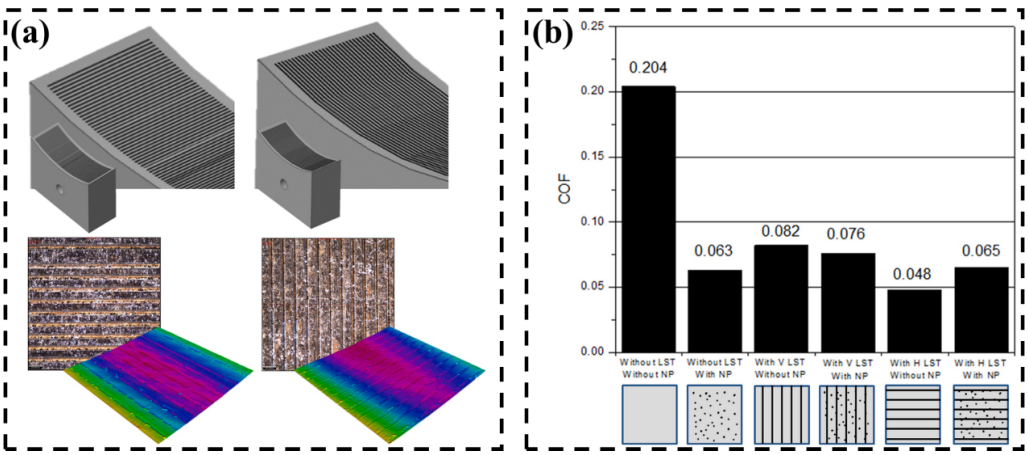

Fig. 25 Surface texture + NP composite treatment method: (a) texture perpendicular to sliding direction (left) and texture parallel to sliding direction (right); (b) average COFs of all texture and NP combinations. Reproduced with permission from Ref. [162], © Elsevier B.V. 2019.

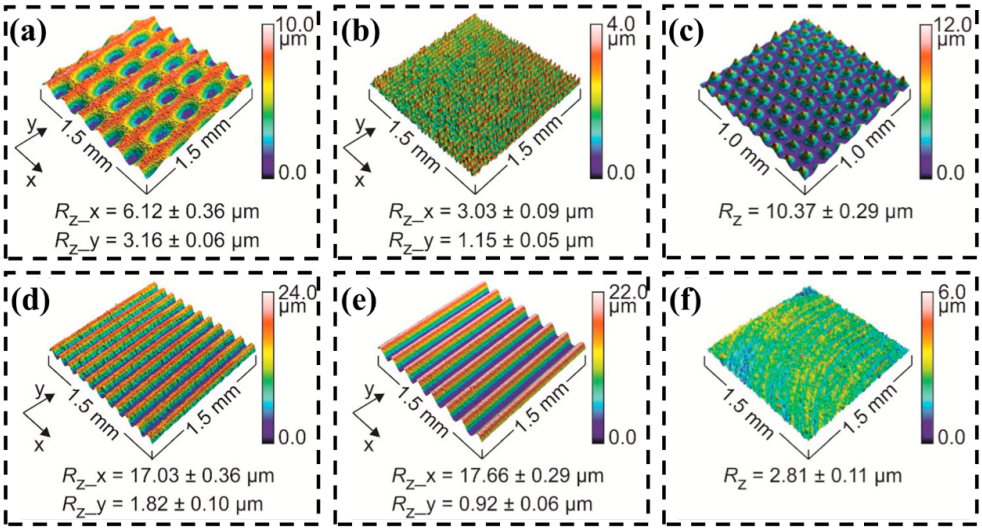

Fig. 26 (a–e) Biomimetic textures; (f) its reference surface. Note: R_z, $R_z(x)$, and $R_z(y)$ are the total mean roughness, mean roughness at the x axis, and mean roughness at the y axis, respectively. Reproduced with permission from Ref. [164], © Elsevier Ltd. 2017.

studying the friction phenomenon, law, and mechanism of AADD were reported. After that, in order to deeply explore the internal mechanism of AADD friction, typical deep drawing friction models in the past two decades were summarized. According to the different model construction methods, they were subdivided into five categories, including single-factor friction model, multi-factor coupled friction model, macro-scale friction model, micro-scale friction model, and multi-scale friction model. Next, two AADD friction simulation methods were introduced. The constant COF simulation was based on Coulomb's law, and the variable COF simulation was based on friction model. Finally, we investigated the application of lubrication-free technologies such as solid lubrication, texture, coating, and composite treatment in the control of AADD friction.

As stated above, a significant progress in AADD friction has been achieved over the past few decades. However, there are still a few great challenges. The first challenge is lack of systematic research on cryogenic temperature AADD friction. It is well-known that the strength and toughness of aluminium alloys generally increase at cryogenic temperatures. The elongation at break in liquid nitrogen (−196 °C) is even 100% higher than that at room temperature. As a transformative technology different from traditional cold and hot forming, cryogenic temperature AADD has gradually drawn much attention since 2015. However, cryogenic temperature AADD friction is rarely mentioned in previously published papers. This is mainly because the accuracy of temperature control of cryogenic medias, such as liquid nitrogen, liquid argon, and liquid helium, is not high. Cryogenic medias are difficult to provide a stable cryogenic environment. And force sensors are unable to function normally under these conditions. Therefore, it is necessary to develop a new COF measurement method suitable for cryogenic temperature AADD. On this basis, the development of AADD friction model, friction simulation, and friction control will also face significant transformations.

The second challenge is the insufficient development of AADD theoretical friction model and variable COF simulation. At present, there are few theoretical friction models based on aluminium alloys, and the existing ones mainly focus on macro-scale friction models. But micro-scale friction models and multi-scale friction models are almost all based on steel. Due to significant differences between aluminium and steel, it is obviously unreasonable to directly apply the friction model based on steel to AADD. At least, the relevant material properties need to be replaced with aluminium alloys. In addition, the grain size and oxides affect the mechanical properties of aluminium alloys at the micro level. The aluminium chips produced by friction adhere to die surface and change the geometry of asperities. The accurate calculation

of COF is inseparable from these factors. Until now, they have not been well integrated into the AADD friction model. Because of various deficiencies in the theoretical friction model of AADD, the development of variable COF simulation is greatly restricted.

The third challenge is how to improve the reliability and stability of lubrication-free AADD friction control. Studies have shown that reasonable friction distribution design in AADD is essential for improving the forming limit of parts, maintaining a uniform wall thickness, and avoiding wrinkling and cracking defects. In the lubrication-free method, solid lubrication and coating mainly contribute to "friction reduction", whereas different surface texture can achieve both "friction reduction" and "friction increase". The combination of the three further strengthens the surface texture regulatory effect. However, the reality has proved that these friction control methods are fragile. They are prone to failure due to breakage under severe deep drawing conditions, and large-area coating, texture processing, and manufacturing costs are high. How to balance the above contradictions and prepare a stable, long-lasting, and wear-resistant surface has become the central issue that AADD lubrication-free technology needs to break through in the future.

To address the aforementioned challenges, more continuous efforts and more cooperation especially with researchers working in the fields of tribology, material science, mechanics, physics, and chemistry are required. All in all, it is an inevitable trend of sustainable development for high-performance aluminium alloys to replace conventional steel. AADD friction is a key boundary condition for controlling the forming quality of parts. Its friction law, test method, friction model, and friction control researches show great application potential. The progress and development in this field will continue to attract global attention.

Acknowledgements

The authors greatly appreciate the financial support by the National Natural Science Foundation of China (11502044, U1906233, and 52175289), the Fundamental Research Funds for the Central Universities (DUT17RC (3)104), and the National Key R&D Program of China (2018YFA0703 and 2019YFA0708804). We also thank Professor Shijian YUAN and Professor Jun YAN, working at Dalian University of Technology, China, for useful discussions and suggestions.

Declaration of competing interest

The authors have no competing interests to declare that are relevant to the content of this article.

References

[1] Schneider R, Grant R J, Schlosser J M, Rimkus W, Radlmayr K, Grabner F, Maier C. An investigation of the deep drawing behavior of automotive aluminium alloys at very low temperatures. *Metall Mater Trans A* **51**(3): 1123–1133 (2020)

[2] Tatipala S, Wall J, Johansson C M, Sigvant M. Data-driven modelling in the era of Industry 4.0: A case study of friction modelling in sheet metal forming simulations. *J Phys Conf Ser* **1063**: 012135 (2018)

[3] Tatipala S, Pilthammar J, Sigvant M, Wall J, Johansson C M. Introductory study of sheet metal forming simulations to evaluate process robustness. *IOP Conf Ser Mater Sci Eng* **418**: 012111 (2018)

[4] Veldhuis M, Heingärtner J, Krairi A, Waanders D, Hazrati J. An industrial-scale cold forming process highly sensitive to temperature induced frictional start-up effects to validate a physical based friction model. *Procedia Manuf* **47**: 578–585 (2020)

[5] Krairi A, Marmi J, Gastebois S, Veldhuis M, Kott M. A speed-up method for numerical simulations of multi-strokes cold metallic sheet forming processes. *Procedia Manuf* **47**: 570–577 (2020)

[6] Kalpakjian S. Recent progress in metal forming tribology. *J Appl Metalworking* **4**(3): 270–280 (1986)

[7] Kawai N, Dohda K. Development of tribology in metal forming. *JSME Int J* **30**(265): 1018–1025 (1987)

[8] Guo L, Li G Y, Zhong Z H, Chen F Z. Advances in friction models of computer simulation of stamping of sheet metal. *China Mechanical Engineering* **14**(21): 1879–1882 (2003) (in Chinese)

[9] Meng L F, Hu C L, Zhao Z. Research progress of friction model in metal plastic forming. *Die & Mould Industry* **40**(4): 1–7 (2014) (in Chinese)

[10] Seshacharyulu K, Bandhavi C, Naik B B, Rao S S, Singh S K. Understanding friction in sheet metal forming—A review. *Mater Today* **5**(9): 18238–18244 (2018)

[11] Xu N, Wang P, Xia J S, Zhang Z Y. Research progress of friction characteristics in plastic forming. *Hot Work Technol* **47**(23): 5–11 (2018) (in Chinese)

[12] Nielsen C V, Bay N. Review of friction modeling in metal forming processes. *J Mater Process Tech* **255**: 234–241 (2018)

[13] Bowden F P, Tabor D. Mechanism of metallic friction. *Nature* **150**(3798): 197–199 (1942)

[14] Li G, Long X Y, Yang P, Liang Z K. Advance on friction of stamping forming. *Int J Adv Manuf Tech* **96**(1–4): 21–38 (2018)

[15] Trzepiecinski T, Lemu H G. Recent developments and trends in the friction testing for conventional sheet metal forming and incremental sheet forming. *Metals* **10**(1): 47 (2020)

[16] Groche P, Callies T. Tribology in sheet metal forming with regard to challenges in lightweight construction. *Adv Mater Res* **6–8**: 93–100 (2005)

[17] Westlund V, Heinrichs J, Jacobson S. On the role of material transfer in friction between metals: Initial phenomena and effects of roughness and boundary lubrication in sliding between aluminium and tool steels. *Tribol Lett* **66**(3): 97 (2018)

[18] Bouchaâla K, Ghanameh M F, Faqir M, Mada M, Essadiqi E. Evaluation of the effect of contact and friction on deep drawing formability analysis for lightweight aluminium lithium alloy using cylindrical cup. *Procedia Manuf* **46**: 623–629 (2020)

[19] Reddy G C M, Reddy P V R R, Reddy T A J. Finite element analysis of the effect of coefficient of friction on the drawability. *Tribol Int* **43**(5–6): 1132–1137 (2010)

[20] Folle L F, Schaeffer L. Effect of surface roughness and lubrication on the friction coefficient in deep drawing processes of aluminium alloy AA1100 with FEM analysis. *Matéria* (*Rio de Janeiro*) **24**(1): e-12298 (2019)

[21] Bellini C, Giuliano G, Sorrentino L. Friction influence on the AA6060 aluminium alloy formability. *Fracture and Structural Integrity* **13**(49): 791–799 (2019)

[22] Ma W Y, Wang B Y, Fu L, Zhou J, Huang M D. Effect of friction coefficient in deep drawing of AA6111 sheet at elevated temperatures. *T Nonferr Metal Soc* **25**(7): 2342–2351 (2015)

[23] Mohamed M, Farouk M, Elsayed A, Shazly M, Hegazy A A. An investigation of friction effect on formability of AA 6061-T4 sheet during cold forming condition. *AIP Conf Proc* **1896**(1): 080025 (2017)

[24] Lu J, Song Y L, Hua L, Zhou P, Xie G J. Effect of temperature on friction and galling behavior of 7075 aluminium alloy sheet based on ball-on-plate sliding test. *Tribol Int* **140**: 105872 (2019)

[25] Lu J, Song Y L, Zhou P, Lin J G, Dean T A, Liu P. Process parameters effect on high-temperature friction and galling characteristics of AA7075 sheets. *Mater Manuf Process* **36**(8): 967–978 (2021)

[26] Hanna M D. Tribological evaluation of aluminium and magnesium sheet forming at high temperatures. *Wear* **267**(5–8): 1046–1050 (2009)

[27] Gali O A, Riahi A R, Alpas A T. The tribological behaviour of AA5083 alloy plastically deformed at warm forming temperatures. *Wear* **302**(1–2): 1257–1267 (2013)

[28] Liu Y, Zhu Z J, Wang Z J, Zhu B, Wang Y L, Zhang Y S. Flow and friction behaviors of 6061 aluminium alloy at elevated temperatures and hot stamping of a B-pillar. *Int J Adv Manuf Tech* **96**(9): 4063–4083 (2018)

[29] Dou S S, Wang X P, Xia J, Wilson L. Analysis of sheet metal forming (warm stamping process): A study of the variable friction coefficient on 6111 aluminium alloy. *Metals* **10**(9): 1189 (2020)

[30] Grabner F, Gruber B, Schlögl C, Chimani C. Cryogenic sheet metal forming—An overview. *Mater Sci Forum* **941**: 1397–1403 (2018)

[31] Sotirov N, Falkinger G, Grabner F, Schmid G, Schneider R, Grant R J, Kelsch R, Radlmayr K, Scheerer M, Reichl C, et al. Improved formability of AA5182 aluminium alloy sheet at cryogenic temperatures. *Mater Today* **2**: S113–S118 (2015)

[32] Kumar M, Sotirov N, Grabner F, Schneider R, Mozdzen G. Cryogenic forming behaviour of AW-6016-T4 sheet. *T Nonferr Metal Soc* **27**(6): 1257–1263 (2017)

[33] Reichl C, Schneider R, Hohenauer W, Grabner F, Grant R J. A numerical simulation of thermodynamic processes for

cryogenic metal forming of aluminium sheets and comparison with experimental results. *Appl Therm Eng* **113**: 1228–1241 (2017)

[34] Wang C G, Yi Y P, Huang S Q, Dong F, He H L, Huang K, Jia Y Z. Experimental and theoretical investigation on the forming limit of 2024-O aluminium alloy sheet at cryogenic temperatures. *Met Mater Int* **27**(12): 5199–5211 (2021)

[35] Padmini B V, Sampathkumaran P, Seetharamu S, Naveen G J, Niranjan H B. Investigation on the wear behaviour of aluminium alloys at cryogenic temperature and subjected to cryo-treatment. *IOP Conf Ser Mater Sci Eng* **502**: 012191 (2019)

[36] Lin J F, Wang L Y, Huang T K. Friction in deep drawing of aluminium sheet. *Wear* **156**(1): 189–199 (1992)

[37] Ooki K, Takahashi S. Investigation of high speed friction test for aluminium alloys. *J Phys Conf Ser* **734**: 032040 (2016)

[38] Hwang Y M, Chen C C. Investigation of effects of strip metals and relative sliding speeds on friction coefficients by reversible strip friction tests. *Metals* **10**(10): 1369 (2020)

[39] Sabet A S, Domitner J, Öksüz K I, Hodžić E, Torres H, Ripoll M R, Sommitsch C. Tribological investigations on aluminium alloys at different contact conditions for simulation of deep drawing processes. *J Manuf Process* **68**: 546–557 (2021)

[40] Steiner J, Merklein M. Investigation of influencing parameters for tribological conditions in dry forming processes. *Acta Metall Sin-Engl* **28**(12): 1435–1441 (2015)

[41] Gil I, Mendiguren J, Galdos L, Mugarra E, de Argandoña E S. Influence of the pressure dependent coefficient of friction on deep drawing springback predictions. *Tribol Int* **103**: 266–273 (2016)

[42] De Argandoña E S, Mendiguren J, Otero I, Mugarra E, Otegi N, Galdos L. Improving the prediction of the final part geometry in high strength steels U drawing by means of advanced material and friction models. *AIP Conf Proc* **1960**(1): 170014 (2018)

[43] Domitner J, Silvayeh Z, Sabet A S, Öksüz K I, Pelcastre L, Hardell J. Characterization of wear and friction between tool steel and aluminium alloys in sheet forming at room temperature. *J Manuf Process* **64**: 774–784 (2021)

[44] Yang X, Liu X C, Liu H L, Politis D J, Leyvraz D, Wang L L. Experimental and modelling study of friction evolution and lubricant breakdown behaviour under varying contact conditions in warm aluminium forming processes. *Tribol Int* **158**: 106934 (2021)

[45] Shi Z, Wang L, Mohamed M, Balint D S, Lin J, Stanton M, Watson D, Dean T A. A new design of friction test rig and determination of friction coefficient when warm forming an aluminium alloy. *Procedia Eng* **207**: 2274–2279 (2017)

[46] Hartfield-Wunsch S E, Cohen D, Sanchez L R, Brattstrom L E. The effect of surface finish on aluminium sheet friction behavior. *SAE Int J Mater Manuf* **4**(1): 818–825 (2011)

[47] Zhou R, Cao J, Wang Q J, Meng F M, Zimowski K, Xia Z C. Effect of EDT surface texturing on tribological behavior of aluminium sheet. *J Mater Process Tech* **211**(10): 1643–1649 (2011)

[48] Keum Y T, Wagoner R H, Lee J K. Friction model for FEM simulation of sheet metal forming operations. *AIP Conf Proc* **712**: 989–994 (2004)

[49] Lemu H G, Trzepieciński T. Numerical and experimental study of frictional behavior in bending under tension test. *Stroj Vestn-J Mech E* **59**(1): 41–49 (2013)

[50] Horiuchi T, Yoshihara S, Iriyama Y. Dry deep drawability of A5052 aluminium alloy sheet with DLC-coating. *Wear* **286–287**: 79–83 (2012)

[51] Abraham T, Bräuer G, Kretz F, Groche P. Observation of the a-C:H run-in behaviour for dry forming applications of aluminium. *MATEC Web Conf* **190**: 14001 (2018)

[52] Tenner J, Andreas K, Radius A, Merklein M. Numerical and experimental investigation of dry deep drawing of aluminium alloys with conventional and coated tool surfaces. *Procedia Eng* **207**: 2245–2250 (2017)

[53] Steiner J, Andreas K, Merklein M. Investigation of surface finishing of carbon based coated tools for dry deep drawing of aluminium alloys. *IOP Conf Ser Mater Sci Eng* **159**: 012022 (2016)

[54] Aktürk D A, Liu P Z, Cao J, Wang Q J, Xia Z C, Talwar R, Grzina D, Merklein M. Friction anisotropy of aluminium 6111-T4 sheet with flat and laser-textured D2 tooling. *Tribol Int* **81**: 333–340 (2015)

[55] Liu X J, Liewald M, Becker D. Effects of rolling direction and lubricant on friction in sheet metal forming. *J Tribol* **131**(4): 042101 (2009)

[56] Saha P K, Wilson W R D, Timsit R S. Influence of surface topography on the frictional characteristics of 3104 aluminium alloy sheet. *Wear* **197**(1–2): 123–129 (1996)

[57] Menezes P L, Kishore, Kailas S V. Studies on friction and transfer layer: Role of surface texture. *Tribol Lett* **24**(3): 265–273 (2006)

[58] Menezes P L, Kishore, Kailas S V. Influence of surface texture and roughness parameters on friction and transfer layer formation during sliding of aluminium pin on steel plate. *Wear* **267**(9–10): 1534–1549 (2009)

[59] Zabala A, Galdos L, Childs C, Llavori I, Aginagalde A, Mendiguren J, de Argandoña E S. The interaction between the sheet/tool surface texture and the friction/galling behaviour on aluminium deep drawing operations. *Metals* **11**(6): 979 (2021)

[60] Hu Y, Zheng Y, Politis D J, Masen M A, Cui J, Wang L. Development of an interactive friction model to predict aluminium transfer in a pin-on-disc sliding system. *Tribol Int* **130**: 216–228 (2019)

[61] Wilson W R D, Sheu S. Real area of contact and boundary friction in metal forming. *Int J Mech Sci* **30**(7): 475–489 (1988)

[62] Zhao R, Steiner J, Andreas K, Merklein M, Tremmel S. Investigation of tribological behaviour of a-C:H coatings for dry deep drawing of aluminium alloys. *Tribol Int* **118**: 484–490 (2018)

[63] Afshin E, Kadkhodayan M. An experimental investigation into the warm deep-drawing process on laminated sheets under various grain sizes. *Mater Design* **87**: 25–35 (2015)

[64] Kirkhorn L, Bushlya V, Andersson M, Ståhl J E. The influence of tool steel microstructure on friction in sheet metal forming. *Wear* **302**(1–2): 1268–1278 (2013)

[65] Meiler M, Jaschke H. Lubrication of aluminium sheet metal within the automotive industry. *Adv Mater Res* **6–8**: 551–558 (2005)

[66] Dyja K, Więckowski W. The effects of friction on stamping process of sheet metals used in aviation. *Arch Metall Mater* **60**(3): 1895–1900 (2015)

[67] Luo Y J, Wang R, He D N, Zhang Y Q. Determination of friction coefficient in sheet metal deep drawing. *J Shanghai JiaoTong Univ* **35**(7): 969–971, 976 (2001) (in Chinese)

[68] Guo Z H, Li Z G, Huang C J, Dong X H. Research on the friction model for lubricated aluminium alloy sheet forming simulation. *China Mech Eng* **15**(15): 1388–1391 (2004) (in Chinese)

[69] Recklin V, Dietrich F, Groche P. *In-situ*-measurement of the friction coefficient in the deep drawing process. *J Phys Conf Ser* **896**: 012027 (2017)

[70] Wang W R, Zhao Y Z, Wang Z M, Hua M, Wei X C. A study on variable friction model in sheet metal forming with advanced high strength steels. *Tribol Int* **93**: 17–28 (2016)

[71] Dong Y C, Zheng K L, Fernandez J, Li X Y, Dong H S, Lin J G. Experimental investigations on hot forming of AA6082 using advanced plasma nitrocarburised and CAPVD WC:C coated tools. *J Mater Process Tech* **240**: 190–199 (2017)

[72] Liewald M, Tovar G E M, Woerz C, Umlauf G. Tribological conditions using CO_2 as volatile lubricant in dry metal forming. *Int J Pr Eng Man-GT* **7**(5): 965–973 (2020)

[73] Han S S. The influence of tool geometry on friction behavior in sheet metal forming. *J Mater Process Tech* **63**(1–3): 129–133 (1997)

[74] Kirkhorn L, Frogner K, Andersson M, Ståhl J E. Improved tribotesting for sheet metal forming. *Procedia CIRP* **3**: 507–512 (2012)

[75] Trzepieciński T, Lemu H G. Proposal for an experimental-numerical method for friction description in sheet metal forming. *Stroj Vestn-J Mech E* **61**(6): 383–391 (2015)

[76] Sanchez L R. Experimental investigation of friction effects enhanced by tool geometry and forming method on plane strain sheet metal forming. *Tribol Trans* **42**(2): 343–352 (1999)

[77] Fratini L, Casto S L, Valvo E L. A technical note on an experimental device to measure friction coefficient in sheet metal forming. *J Mater Process Tech* **172**(1): 16–21 (2006)

[78] Saha P K, Wilson W R D. Influence of plastic strain on friction in sheet metal forming. *Wear* **172**(2): 167–173 (1994)

[79] Bay N, Olsson D D, Andreasen J L. Lubricant test methods for sheet metal forming. *Tribol Int* **41**(9–10): 844–853 (2008)

[80] Andreasen J L, Olsson D D, Chodnikiewicz K, Bay N. Bending under tension test with direct friction measurement. *P I Mech Eng B-J Eng* **220**(1): 73–80 (2006)

[81] Ramezani M, Neitzert T, Pasang T, Sellès M A. Characterization of friction behaviour of AZ80 and ZE10 magnesium alloys under lubricated contact condition by strip draw and bend test. *Int J Mach Tool Manu* **85**: 70–78 (2014)

[82] Reichardt G, Liewald M. Investigation on friction behaviour of deep drawing radii using volatile media as lubricant substitutes. *Procedia Manuf* **29**: 193–200 (2019)

[83] Trzepiecinski T. A study of the coefficient of friction in steel sheets forming. *Metals* **9**(9): 988 (2019)

[84] Hao S, Klamecki B E, Ramalingam S. Friction measurement apparatus for sheet metal forming. *Wear* **224**(1): 1–7 (1999)

[85] Dilmec M, Arap M. Effect of geometrical and process parameters on coefficient of friction in deep drawing process at the flange and the radius regions. *Int J Adv Manuf Tech* **86**(1): 747–759 (2016)

[86] Evin E, Tomáš M. Tribology properties evaluation for friction pair Zn coated steel–TiCN MP coated/uncoated tool steel. *Acta Metall Slovaca* **25**(4): 208–216 (2019)

[87] Dou S S, Xia J S. Analysis of sheet metal forming (stamping process): A study of the variable friction coefficient on 5052 aluminium alloy. *Metals* **9**(8): 853 (2019)

[88] Klocke F, Trauth D, Shirobokov A, Mattfeld P. FE-analysis and *in situ* visualization of pressure-, slip-rate-, and temperature-dependent coefficients of friction for advanced sheet metal forming: Development of a novel coupled user subroutine for shell and continuum discretization. *Int J Adv Manuf Tech* **81**(1): 397–410 (2015)

[89] Zhou D, Yuan X, Gao H X, Wang A L, Liu J, El Fakir O, Politis D J, Wang L L, Lin J G. Knowledge based cloud FE simulation of sheet metal forming processes. *J Vis Exp* (118): 53957 (2016)

[90] Tamai Y, Inazumi T, Manabe K I. FE forming analysis with nonlinear friction coefficient model considering contact pressure, sliding velocity and sliding length. *J Mater Process Tech* **227**: 161–168 (2016)

[91] Tabor D. Junction growth in metallic friction: The role of combined stresses and surface contamination. *P Roy Soc A-Math Phy* **251**(1266): 378–393 (1959)

[92] Leu D K. A simple dry friction model for metal forming process. *J Mater Process Tech* **209**(5): 2361–2368 (2009)

[93] Ramezani M, Ripin Z M. A friction model for dry contacts during metal-forming processes. *Int J Adv Manuf Tech* **51**(1–4): 93–102 (2010)

[94] Gearing B P, Moon H S, Anand L. A plasticity model for interface friction: Application to sheet metal forming. *Int J Plasticity* **17**(2): 237–271 (2001)

[95] Wilson W R D, Hsu T C, Huang X B. A realistic friction model for computer simulation of sheet metal forming processes. *J Eng Ind* **117**(2): 202–209 (1995)

[96] Darendeliler H, Akkök M, Ali Yücesoy C. Effect of variable friction coefficient on sheet metal drawing. *Tribol Int* **35**(2): 97–104 (2002)

[97] Yang T S. Investigation of the strain distribution with lubrication during the deep drawing process. *Tribol Int* **43**(5–6): 1104–1112 (2010)

[98] Başpınar M, Akkök M. Modeling and simulation of friction in deep drawing. *J Tribol* **138**(2): 021104 (2016)

[99] Sojoudi H, Khonsari M M. On the modeling of quasi-steady and unsteady dynamic friction in sliding lubricated line contact. *J Tribol* **132**(1): 012101 (2010)

[100] Zhao Y W, Maietta D M, Chang L. An asperity microcontact model incorporating the transition from elastic deformation to fully plastic flow. *J Tribol* **122**(1): 86–93 (2000)

[101] Karupannasamy D K, Hol J, de Rooij M B, Meinders T, Schipper D J. A friction model for loading and reloading effects in deep drawing processes. *Wear* **318**(1–2): 27–39 (2014)

[102] De Rooij M B, van der Linde G, Schipper D J. Modelling material transfer on a single asperity scale. *Wear* **307**(1–2): 198–208 (2013)

[103] Mishra T, de Rooij M, Shisode M, Hazrati J, Schipper D J. Analytical, numerical and experimental studies on ploughing behaviour in soft metallic coatings. *Wear* **448–449**: 203219 (2020)

[104] Mishra T, de Rooij M, Shisode M, Hazrati J, Schipper D J. Characterization of interfacial shear strength and its effect on ploughing behaviour in single-asperity sliding. *Wear* **436–437**: 203042 (2019)

[105] Mishra T, Ganzenmüller G C, de Rooij M, Shisode M, Hazrati J, Schipper D J. Modelling of ploughing in a single-asperity sliding contact using material point method. *Wear* **418–419**: 180–190 (2019)

[106] Mishra T, de Rooij M, Shisode M, Hazrati J, Schipper D J. An analytical model to study the effect of asperity geometry on forces in ploughing by an elliptical asperity. *Tribol Int* **137**: 405–419 (2019)

[107] Shisode M, Hazrati J, Mishra T, de Rooij M, ten Horn C, van Beeck J, van den Boogaard T. Modeling boundary friction of coated sheets in sheet metal forming. *Tribol Int* **153**: 106554 (2021)

[108] Hol J, Meinders V T, de Rooij M B, van den Boogaard A H. Multi-scale friction modeling for sheet metal forming: The boundary lubrication regime. *Tribol Int* **81**: 112–128 (2015)

[109] Mishra T, de Rooij M, Shisode M, Hazrati J, Schipper D J. A material point method based ploughing model to study the effect of asperity geometry on the ploughing behaviour of an elliptical asperity. *Tribol Int* **142**: 106017 (2020)

[110] Bowden F P, Moore A J W, Tabor D. The ploughing and adhesion of sliding metals. *J Appl Phys* **14**(2): 80–91 (1943)

[111] Challen J M, Oxley P L B. An explanation of the different regimes of friction and wear using asperity deformation models. *Wear* **53**(2): 229–243 (1979)

[112] Challen J M, Oxley P L B. Slip-line fields for explaining the mechanics of polishing and related processes. *Int J Mech Sci* **26**(6–8): 403–418 (1984)

[113] Hol J, Alfaro M V C, de Rooij M B, Meinders T. Advanced friction modeling for sheet metal forming. *Wear* **286–287**: 66–78 (2012)

[114] Karupannasamy D K, Hol J, de Rooij M B, Meinders T, Schipper D J. Modelling mixed lubrication for deep drawing processes. *Wear* **294–295**: 296–304 (2012)

[115] Greenwood J A, Williamson J B P. Contact of nominally flat surfaces. *P Roy Soc A-Math Phy* **295**: 300–319 (1966)

[116] Pullen B J, Williamson J B P. On the plastic contact of rough surfaces. *P Roy Soc A-Math Phy* **327**: 159–173 (1972)

[117] Westeneng A J D. Modelling of contact and friction in deep drawing processes. Ph.D. Thesis. Enschede (the Netherlands): University of Twente, 2001.

[118] Hol J, Meinders V T, Geijselaers H J M, van den Boogaard A H. Multi-scale friction modeling for sheet metal forming: The mixed lubrication regime. *Tribol Int* **85**: 10–25 (2015)

[119] Venema J, Hazrati J, Atzema E, Matthews D, van den Boogaard T. Multiscale friction model for hot sheet metal forming. *Friction* **10**(2): 316–334 (2022)

[120] Venema J, Atzema E, Hazrati J, Matthews D, van den Boogaard T. Modelling of friction in hot stamping. *Procedia Manuf* **47**: 596–601 (2020)

[121] Shisode M, Hazrati J, Mishra T, de Rooij M, van den Boogaard T. Mixed lubrication friction model including surface texture effects for sheet metal forming. *J Mater Process Tech* **291**: 117035 (2021)

[122] Shisode M P, Hazrati J, Mishra T, de Rooij M, van den Boogaard T. Modeling mixed lubrication friction for sheet metal forming applications. *Procedia Manuf* **47**: 586–590 (2020)

[123] Nielsen C V, Martins P A F, Bay N. Modelling of real area of contact between tool and workpiece in metal forming processes including the influence of subsurface deformation. *CIRP Ann* **65**(1): 261–264 (2016)

[124] Kayaba T, Kato K. Experimental analysis of junction growth with a junction model. *Wear* **51**(1): 105–116 (1978)

[125] Lo S W, Tsai S D. Real-time observation of the evolution of contact area under boundary lubrication in sliding contact. *J Tribol* **124**(2): 229–238 (2002)

[126] Sutcliffe M P F. Surface asperity deformation in metal forming processes. *Int J Mech Sci* **30**(11): 847–868 (1988)

[127] Shisode M, Hazrati J, Mishra T, de Rooij M, van den Boogaard T. Evolution of real area of contact due to combined normal load and sub-surface straining in sheet metal. *Friction* **9**(4): 840–855 (2021)

[128] Bouchaâla K, Ghanameh M F, Faqir M, Mada M, Essadiqi E. Prediction of the impact of friction's coefficient in cylindrical deep drawing for AA2090 Al–Li alloy using FEM and Taguchi approach. *IOP Conf Ser Mater Sci Eng* **664**(1): 012004 (2019)

[129] Shivpuri R, Zhang W F. Robust design of spatially distributed friction for reduced wrinkling and thinning failure in sheet drawing. *Mater Design* **30**(6): 2043–2055 (2009)

[130] Zabala A, de Argandoña E S, Cañizares D, Llavori I, Otegi N, Mendiguren J. Numerical study of advanced friction modelling for sheet metal forming: Influence of the die local roughness. *Tribol Int* **165**: 107259 (2022)

[131] Wiklund D, Rosén B G, Wihlborg A. A friction model evaluated with results from a bending-under-tension test. *Tribol Int* **42**(10): 1448–1452 (2009)

[132] Wiklund D, Larsson M. Phenomenological friction model in deep drawing of aluminium sheet metals. *IOP Conf Ser Mater Sci Eng* **418**: 012097 (2018)

[133] Bolay C, Essig P, Kaminsky C, Hol J, Naegele P, Schmidt R. Friction modelling in sheet metal forming simulations for aluminium body parts at Daimler AG. *IOP Conf Ser Mater Sci Eng* **651**(1): 012104 (2019)

[134] Durmaz U, Heibel S, Schweiker T, Merklein M, Berahmani S, Hol J, Naegele P. Enhancement of springback prediction of AHSS parts by advanced friction modelling. *IOP Conf Ser Mater Sci Eng* **1157**(1): 012033 (2021)

[135] Chezan A R, Khandeparkar T V, ten Horn C H L J, Sigvant M. Accurate sheet metal forming modeling for cost effective automotive part production. *IOP Conf Ser Mater Sci Eng* **651**(1): 012007 (2019)

[136] Güner A, Hol J, Venema J, Sigvant M, Dobrowolski F, Komodromos A, Tekkaya A E. Application of an advanced friction model in hot stamping simulations: A numerical and experimental investigation of an A-pillar reinforcement panel from Volvo cars. *IOP Conf Ser*: *Mater Sci Eng* **1157**(1): 012020 (2021)

[137] Sigvant M, Pilthammar J, Hol J, Wiebenga J H, Chezan T, Carleer B, van den Boogaard A H. Friction and lubrication modeling in sheet metal forming simulations of a Volvo XC90 inner door. *IOP Conf Ser Mater Sci Eng* **159**: 012021 (2016)

[138] Sigvant M, Pilthammar J, Hol J, Wiebenga J H, Chezan T, Carleer B, van den Boogaard A H. Friction in sheet metal forming: Forming simulations of dies in try-out. *J Phys Conf Ser* **1063**: 012134 (2018)

[139] Sigvant M, Pilthammar J, Hol J, Wiebenga J H, Chezan T, Carleer B, van den Boogaard A H. Friction in sheet metal forming simulations: Modelling of new sheet metal coatings and lubricants. *IOP Conf Ser Mater Sci Eng* **418**: 012093 (2018)

[140] Sigvant M, Pilthammar J, Hol J, Wiebenga J H, Chezan T, Carleer B, van den Boogaard T. Friction in sheet metal forming: Influence of surface roughness and strain rate on sheet metal forming simulation results. *Procedia Manuf* **29**: 512–519 (2019)

[141] Chezan T, Khandeparkar T, van Beeck J, Sigvant M. Strategies for increasing the accuracy of sheet metal forming finite element models. *J Phys Conf Ser* **1063**: 012138 (2018)

[142] Hol J, Wiebenga J H, Hörning M, Dietrich F, Dane C. Advanced friction simulation of standardized friction tests: A numerical and experimental demonstrator. *J Phys Conf Ser* **734**: 032092 (2016)

[143] Hol J, Wiebenga J H, Stock J, Wied J, Wiegand K, Carleer B. Improving stamping simulation accuracy by accounting for realistic friction and lubrication conditions: Application to the door-outer of the Mercedes-Benz C-class Coupé. *J Phys Conf Ser* **734**: 032091 (2016)

[144] Berahmani S, Bilgili C, Erol G, Hol J, Carleer B. The effect of friction and lubrication modelling in stamping simulations of the Ford Transit hood inner panel: A numerical and experimental study. *IOP Conf Ser Mater Sci Eng* **967**: 012010 (2020)

[145] Lacues J, Pan C, Franconville J C, Guillot P, Capellaere M, Chezan T, Hol J, Wiebenga J H, Souchet A, Ferragu V. Friction and lubrication in sheet metal forming simulations: Application to the Renault Talisman trunk lid inner part. *IOP Conf Ser Mater Sci Eng* **651**(1): 012001 (2019)

[146] Waanders D, Marangalou J H, Kott M, Gastebois S, Hol J. Temperature dependent friction modelling: The influence of temperature on product quality. *Procedia Manuf* **47**: 535–540 (2020)

[147] Van Beeck J, Chezan A R, Khandeparkar T V. Advanced tribomechanical modelling of sheet metal forming for the automotive industry. *IOP Conf Ser Mater Sci Eng* **418**: 012096 (2018)

[148] Ghiotti A, Bruschi S, Medea F. Wear onset in hot stamping of aluminium alloy sheets. *Wear* **376–377**(A): 484–495 (2017)

[149] Kamis S L, Lah M A C, Rahama N S, Abd Rahim N A. Fabrication and tribological characterization of aluminium alloy by using photochemical machining. *Jurnal Tribologi* **28**: 82–95 (2021)

[150] Taha-Tijerina J J, Garza G T, Maldonado-Cortés D. Evaluation of parameters for application of Laser Surface Texturing (LST) in tooling for the sheet-metal forming process. *Ind Lubr Tribol* **70**(4): 620–627 (2018)

[151] Costa H L, Hutchings I M. Some innovative surface texturing techniques for tribological purposes. *P I Mech Eng J-J Eng* **229**(4): 429–448 (2015)

[152] Gachot C, Rosenkranz A, Hsu S M, Costa H L. A critical assessment of surface texturing for friction and wear improvement. *Wear* **372–373**: 21–41 (2017)

[153] Flegler F, Neuhäuser S, Groche P. Influence of sheet metal texture on the adhesive wear and friction behaviour of EN AW-5083 aluminium under dry and starved lubrication. *Tribol Int* **141**: 105956 (2020)

[154] Hu T C, Hu L T. The study of tribological properties of laser-textured surface of 2024 aluminium alloy under boundary lubrication. *Lubr Sci* **24**(2): 84–93 (2012)

[155] Murakawa M, Koga N, Kumagai T. Deep-drawing of aluminium sheets without lubricant by use of diamond-like carbon coated dies. *Surf Coat Tech* **76–77**: 553–558 (1995)

[156] Sgarabotto F, Ghiotti A, Bruschi S. Influence of temperature on AA6014 alloy tribological behaviour in stamping operations. *AIP Conf Proc* **1353**(1): 1723–1728 (2011)

[157] Häfner T, Rothammer B, Tenner J, Krachenfels K, Merklein M, Tremmel S, Schmidt M. Adaption of tribological behavior of a-C:H coatings for application in dry deep drawing. *MATEC Web Conf* **190**: 14002 (2018)

[158] Krachenfels K, Rothammer B, Tremmel S, Merklein M. Experimental investigation of tool-sided surface modifications for dry deep drawing processes at the tool radii area. *Procedia Manuf* **29**: 201–208 (2019)

[159] Cai H L, Zhang C, Li H T, Jiang B L. Self-lubricating nanocomposite coatings using MAO to improve tribological properties of 6061 aluminium alloy. *Mater Res Express* **8**(3): 036401 (2021)

[160] Dong Y C, Zheng K L, Fernandez J, Fuentes G, Li X Y, Dong H S. Tribology and hot forming performance of self-lubricious NC/NiBN and NC/WC:C hybrid composite coatings for hot forming die. *J Mater Process Tech* **252**: 183–190 (2018)

[161] Lacki P. Optimisation of the stamping processes for a drawn-part made of aluminium. *Key Eng Mater* **410–411**: 271–278 (2009)

[162] Maldonado-Cortés D, Peña-Parás L, Barrios-Saldaña V, Cruz-Bañuelos J S, Adamiak M. Synergistic effect on the tribological properties of tool steel through the use of laser surface texturing channels and nanoparticles. *Wear* **426–427**(B): 1354–1361 (2019)

[163] Tenner J, Zhao R, Tremmel S, Häfner T, Schmidt M, Merklein M. Tribological behavior of carbon based coatings adapted to lubricant-free forming conditions. *Int J Pr Eng Man-GT* **5**(3): 361–367 (2018)

[164] Tillmann W, Stangier D, Lopes-Dias N F, Biermann D, Krebs E. Adjustment of friction by duplex-treated, bionic structures for Sheet–Bulk Metal Forming. *Tribol Int* **111**: 9–17 (2017)

Yiren GAO. He received his M.S. degree in mechanical engineering in 2020 from Dalian University of Technology, China. Now, he is a Ph.D. candidate in School of Mechanical Engineering, Dalian University of Technology, China. His research interests focus on the friction and lubrication in ultra-low temperature forming of aluminium alloy. He has developed a new cryogenic strip drawing tribometer applied to tribological studies for light alloy forming at ultra-low temperature.

Hongxia LI. She obtained her Ph.D. degree in engineering mechanics from the Dalian University of Technology, China, in 2014. She currently serves as an associate professor in School of Mechanical Engineering at Dalian University of Technology. Her expertise lies in friction theory and structural design optimization.

Danyang ZHAO. He received his Ph.D. degree in mechanical engineering from the Dalian University of Technology, China, in 2007, followed by postdoctoral training at Georgia Institute of Technology from 2011 to 2012. He currently serves as a professor in School of Mechanical Engineering at Dalian University of Technology. His research interests focus on functional surface manufacturing and design. He is the deputy dean of School of Mechanical Engineering, Dalian University of Technology.

Minjie WANG. He obtained his Ph.D. degree in mechanical engineering from the Dalian University of Technology, China, in 1989. He currently serves as a professor in School of Mechanical Engineering at Dalian University of Technology. His expertise lies in mold CAD/CAE/CAM technology. He is the experts in metal forming and elastic–plastic theory. He is the director of Engineering Research Center of Ministry of Education for Molded Products.

Xiaobo FAN. He received his Ph.D. degree in material processing engineering from Harbin Institute of Technology, China, in 2016. He is an associate professor in School of Mechanical Engineering at Dalian University of Technology, China. He is the Youth Editor of *International Journal of Extreme Manufacturing*. He is engaged in the research on the innovative process of ultra-low temperature forming and corresponding mechanism, tool design and deformation simulation under extreme environment, and the collaborative control technology of shape accuracy and structure performance of light alloy thin shells. The research results won the Second Prize of Chinese State Technological Invention Award in 2020. The proposed scientific issue of "physical mechanism of dual enhancement effect at ultra-low temperature" was selected as one of the top ten frontier scientific issues of China Association for Science and Technology in 2021.